POLITECNICO
MILANO 1863

SCUOLA DI INGEGNERIA INDUSTRIALE
E DELL'INFORMAZIONE

Augmented Reality and Robot-Assisted Needle Insertion for Percutaneous Nephrolithotomy Task

Tesi di Laurea Magistrale in
Biomedical Engineering - Ingegneria Biomedica

Author: **Matteo Pecorella**

Student ID: 967727
Advisor: Prof. Elena De Momi
Co-advisors: Junling Fu
Academic Year: 2022-23

Acknowledgements

First and foremost, I would like to thank my advisor, Prof. Elena De Momi, for providing me with the chance to work with a multicultural team on a beautiful research project in an area I enjoy, as well as for her invaluable suggestions and revisions throughout the last year.

I would like to express my sincere gratitude to my co-advisor Junling Fu, whose support, patience, and qualification have been invaluable throughout this process. Junling has consistently demonstrated exceptional professionalism, empathy, and expertise, offering insightful guidance and assistance whenever I needed it.

A special thank you to my girlfriend Sandra Angelovska, who stood by my side through the good and challenging parts of my master's degree and thesis, giving me priceless emotional support, inspiration, and comprehension.

Also, many thanks to Adelaide Stucchi, Gabriele Calamai, Martina Senesi, Andrea Pagliari, Lorenzo Male, Matteo Makovec, Gabriele Morelli, Valentina Oliveri, Francesco Scali, Nicoletta Cortesi, Diego Catta, Matteo Costantini and Sara Candido for graciously agreeing to participate in the user trial and more importantly for being an integral part of my academic journey. Their support and encouragement have helped me achieve my goals and overcome obstacles along the way.

I would also like to express my gratitude to my longtime friends Edward Guarino, Andrea Ferraris, Giuliano Rinaldi, Niccolò D'Agaro, Marco Persegatti, Giacomo Furlan, and Matilde Apollonio for always being a source of strength and motivation for me. I am deeply grateful for their kindness, unwavering loyalty, and constant presence in my life.

Last but not least, heartfelt thanks to Francesca Pecorella, my parents, and my family as a whole for supporting and encouraging me throughout all these years. Without them, all of this would be impossible, not only from the financial point of view but in particular from the emotional and moral standpoint. Their guidance and belief in me have been my rock and inspiration, pushing me to strive for excellence and never give up.

Abstract

Objective: The aim of this work was to evaluate the accuracy (deviation from the target or intended path), efficacy (insertion time), and system usability, of a system implementing Augmented Reality and Robotic assistance for the needle insertion step of percutaneous nephrolithotomy (PCNL) procedure. The PCNL procedure is the gold standard for the treatment of large kidney stones. Accurate needle insertion is crucial for successful surgery, but it's challenging due to the complex imaging and high surgeon workload.
Method: The proposed system implements an Augmented Reality (AR) application combined with a robot assisting the needle insertion. The AR is implemented through the Microsoft HoloLens2 headset and visualizes the patient anatomy 3D model, the target stone and the pre-planned insertion path, registered on the real patient. The robotic assistance is implemented by means of a KUKA LWR 4+ robot running an impedance controller for the surgeon's guidance along the pre-planned path.
The experimental setup included a user test of 14 users performing the same needle insertion task with all the possible setup combinations implementing 2D screen visualization or AR and free hand insertion or robotic-assisted insertion. Moreover, the system usability was assessed by means of the NASA Task Load Index questionnaire.
Results: The mean translation error of the proposed system was 3.2 $\pm$ 1.4 mm and the orientation error was 1.2 $\pm$ 0.9 deg with a mean execution time of 171 $\pm$ 109 s. The accuracy of all the other systems where lower. The lower time of execution of 100 $\pm$ 55 s was reached from the AR with the manual insertion system, while the rest of the other systems' times of execution were comparable. The user questionnaire showed the best usability of the proposed system.
Conclusion: This analysis demonstrated that the system implementing AR and robotic assistance can be used for the execution of percutaneous nephrolithotomy needle insertion with high accuracy with respect to the current standard procedure modality and with respect to the current state of the art in this field. Furthermore, AR visualization and robotic assistance increased the system's usability.

Keywords: Robotic assistance, KUKA LWR 4+, Augmented Reality, Surgery, Percutaneous needle insertion.

Abstract in lingua italiana

Obbiettivo: Lo scopo di questo lavoro era valutare l'accuratezza, l'efficacia e l'usabilità di un sistema che implementa la realtà aumentata e l'assistenza robotica per la fase di inserzione della procedura di nefrolitotomia percutanea (PCNL). La procedura PCNL è lo standard di riferimento per il trattamento dei grossi calcoli renali. L'inserimento accurato dell'ago è fondamentale per un intervento chirurgico di successo, ma risulta complesso a causa della tecnica di imaging e dell'elevato carico di lavoro del chirurgo.
Metodo: Il sistema proposto implementa un'applicazione di Realtà Aumentata (RA) combinata con un robot che assiste l'inserimento dell'ago. La RA è implementata attraverso gli occhiali Microsoft HoloLens2 e visualizza il modello 3D dell'anatomia del paziente, il calcolo renale e il percorso di inserimento pre-programmato, registrato sul paziente reale. L'assistenza robotica viene implementata tramite un robot KUKA LWR 4+ in controllo ad impedenza per la guida del chirurgo lungo il percorso pre-programmato. Durante la fase di test, sono stati condotti user test con 14 partecipanti che hanno eseguito la stessa attività di inserzione, utilizzando tutte le possibili configurazioni implementate, tra cui la visualizzazione su schermo 2D o RA e l'inserimento manuale o assistito. Inoltre, l'usabilità del sistema è stata valutata mediante il questionario NASA Task Load Index.
Risultati: Gli errori di traslazione e orientamento medi del sistema proposto erano di 3,2 $\pm$ 1,4 mm e 1,2 $\pm$ 0,9 gradi rispettivamente con un tempo medio di esecuzione di 171 $\pm$ 109 s. La precisione di tutti gli altri sistemi era inferiore. Il minor tempo di esecuzione di 100 $\pm$ 55 s è stato raggiunto dal sistema con RA e sistema di inserimento manuale, mentre gli altri tempi di esecuzione erano comparabili. Il questionario ha evidenziato la migliore usabilità del sistema proposto.
Conclusioni: Questa analisi ha dimostrato che il sistema che implementa la RA e l'assistenza robotica può essere utilizzato per l'esecuzione dell'inserione della PCNL con elevata precisione rispetto alla modalità di procedura standard e rispetto all'attuale stato dell'arte in questo campo. Inoltre, la visualizzazione in RA e l'assistenza robotica hanno aumentato l'usabilità del sistema.

Parole chiave: Assistenza robotica, KUKA LWR 4+, Realtà Aumentata, Chirurgia, nefrolitotomia percutanea.

Contents

Introduction

Pecutaneous Nephrolithotomy The following work operates in the field of Percutaneous Nephrolithotomy (PCNL) which, according to the European and the American Urological Associations, is considered the gold standard procedure for the treatment of patients with renal stones larger than 20mm in diameter [1].

Originally the treatment for patients with renal calculi was based on passing a rigid cystoscope into the kidney during open surgery. The evolution of the procedure lead to the implementation of a percutaneous nephrostomy under radiological control that brought the advantages of the minimally invasive procedure such as minimization of incision size, pain, blood loss, and therefore shortened hospitalization [2]. In the following developments, there was an improvement in the procedure with the substitution of the rigid cystoscope with a nephroscope, the improvement of the radiological imaging thanks to fluoroscopy, and the improvement of stones fragmentation with lasers that lead to the current Percutaneous Nephrolithotomy method [3].

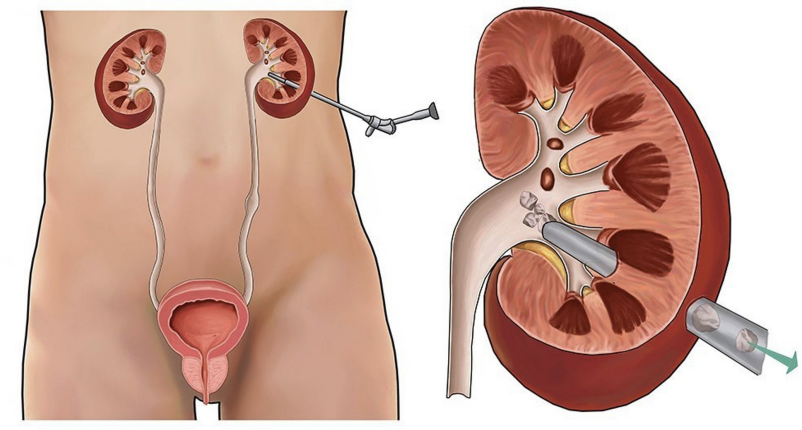

Figure 1: PCNL's positioning of the nephroscope in the renal calyx

The procedure consists on the insertion of the nephroscope into the calyx of the kidney, as shown in Fig 1, at the level of the location of the stone, followed by the emission of

ultrasounds or a laser beam to break the stone apart and suction the small pieces out through one of the channels of the scope. The thin insertion track, of around 1cm in diameter, is previously created in the patient's lower flank or abdomen using a hollow needle insertion guided by fluoroscopy and ultrasonic imaging [4].

The best surgery outcome in terms of patient safety, time consumption, and stone removal, is achieved if the needle insertion position and orientation are as accurate as possible since a bad insertion path could lead to harm to some organs such as the large intestine or the vessels or even to the impossibility to reach the stone. Thus, renal access is a crucial aspect in PCNL [4].

Despite the improvements in the procedure, there are still some limitations such as the surgeon's workload and the challenge of precise needle insertion. The surgeon, in fact, needs to handle several jobs simultaneously, as shown in Fig 2, such as coordination with an interventional radiologist and nurses, monitoring the ultrasonic images for spotting the soft tissues positions that have to be avoided, and deal with other tasks simultaneously like viewing CT images taken prior operation to identify the ureter position [5]. Due to the cruciality of the task and the difficulty of hand-eye coordination for the surgeon in placing the needle looking at the radiological images on the screen, this step results to be challenging with a very steep learning curve. In fact, it has been demonstrated that a surgeon with no previous experience in performing PCNL requires 45 and 105 operations to achieve competence and excellence [6].

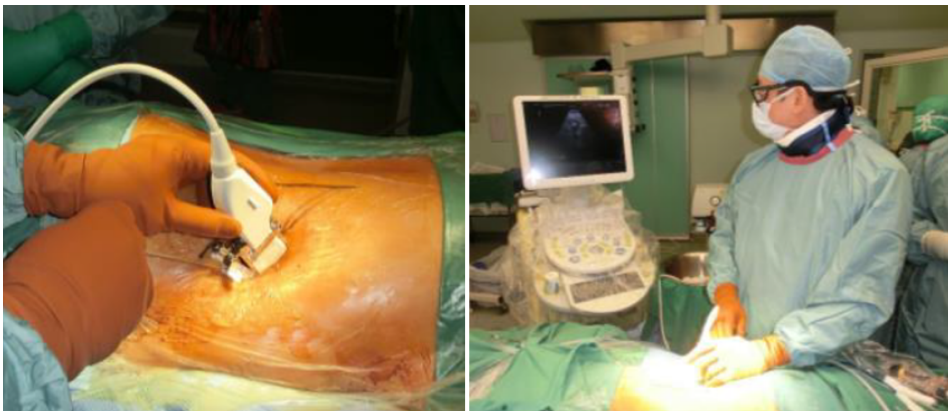

Figure 2: PCNL's surgeon workload

Alongside the complexity of the procedure, there is an additional limitation for the standard PCNL which is the high number of CT-scans acquisitions needed to locate the ureter and needle updated positions in the patient body. This imaging method exposes the peo-

ple in the operating room to dangerous radiation.

Robotics in surgery The rapid progress in computer technology, telecommunications, and electronics has drastically transformed our methods of communication and daily operations, whether it be at work or in our personal lives. These advancements have led to the development of automated tools, machinery, and robotics that have significantly enhanced efficiency in accomplishing tasks, conducting business, and improving overall productivity. Furthermore, the field of medicine has also benefited from such technological breakthroughs. Robotics, which was previously utilized mainly in manufacturing products, space exploration, and underwater applications, has now advanced into the operating room to aid in less complicated surgical procedures. During the 1980s, the medical community began exploring the use of robots in neurosurgery and orthopedic surgery. Early successes with these devices included precise stereotactic localization in neurosurgery and efficient reaming of the femur shaft for prosthetic hip surgery. These achievements generated interest in other fields such as urology.

In more recent years, as surgery shifts toward less invasive procedures, laparoscopic and robotic techniques have gained popularity. Laparoscopy in fact has decreased scarring and hospitalization time, although it has also limited surgeon's dexterity, sensory feedback, and visualization compared to open surgery. However, the development of surgical robotic systems has addressed these limitations, making minimally invasive robotic-assisted surgery (RAS) a promising area for integrating technological advancements into traditional minimally invasive surgery (figure 3).
As laparoscopy gains ground, there has been a push to develop surgical systems that deploy laparoendoscopic single-port surgery (LESS) instruments. Additionally, natural orifice transluminal endoscopic surgery (NOTES) has become popular, and developers are working on producing congruent robotic platforms. The master and slave transluminal endoscopic robot (MASTER) platform seeks to expand user control dexterity, instrument sensory feedback, and location triangulation, which could increase procedural capabilities in NOTES [7].
Surgeons are continually searching for procedures and technology to improve outcomes and leave patients with no visible scars, supporting these efforts.

(a) Manual laparoscopic procedure (b) RAS laparoscopy

Figure 3: Robotics spread in laparoscopy procedures

Augmented Reality in surgery In the years, the role of imaging has become increasingly important in many areas of surgery, and it has been around since 1895 when X-rays were discovered. While X-rays have become more widely used over the years, other techniques have also been developed for acquiring data from inside the human body. This has led to the development of image-guided surgery (IGS), which uses images to guide surgeons during interventions. In recent years, solutions such as 3D visualization and augmented reality (AR) have been used to support physicians in the diagnosis, preoperative phase, and surgeries themselves. AR involves merging virtual objects with the real world, and it has been used in medicine since 1968. Unlike virtual reality (VR), which creates a digital environment, AR overlays computer-generated images onto the real world. The application of AR in IGS can be beneficial for patients as it allows doctors to see 3D images projected directly onto them using special displays. This can improve the perception of the reality examined and make it easier for doctors compared to using traditional 2D preoperative images on 2D monitors that require mental transformation into 3D objects and take the doctor's sight away from the patient [8].

The main aspects of visualizing virtual objects superimposed on the real world using augmented reality systems are: tracking and registration. Tracking is the process of determining the device's location and orientation within the environment, while registration is the process of matching the tracked spatial features with corresponding points of the virtual objects to achieve optimal overlapping. The accuracy of the registration process determines the natural appearance of the augmented image. The process can be manual, fully automatic, or semi-automatic, depending on the ways tracking and registration are accomplished.
Various AR display technologies are available to visualize virtual objects in the real world. These technologies are classified into three categories based on their location [9]:

- **World devices**: such as desktop displays and projector-based displays, are fixed in one place. Desktop displays have a webcam, a virtual mirror, and a virtual showcase that show the real-world scene and additional information. Projector-based displays project virtual objects onto real-world objects.
- **Body devices**: like tablets and mobile phones, use cameras and sensors to capture the scene and determine their rotation. Handheld devices usually use fiducial image targets for tracking-registration.
- **Head devices**: Head-mounted displays (HMDs) are wearable devices like glasses that leave the user's hands free for other tasks. HMDs can be video see-through or optical see-through. Video see-through displays let the user see the real world through a camera and combine it with virtual objects. Optical see-through displays use lenses to overlay images from a projector with the real world, allowing the user to visualize the augmented reality directly. Figure 4 is an example of an HMD.

Figure 4: Example of HMD, HoloLens 2 (Microsoft, WA, USA)

Proposed system framework In order to remove the above mentioned limitations, an Augmented-Reality based Robotics-Assistance application has been developed for the PCNL procedure support.

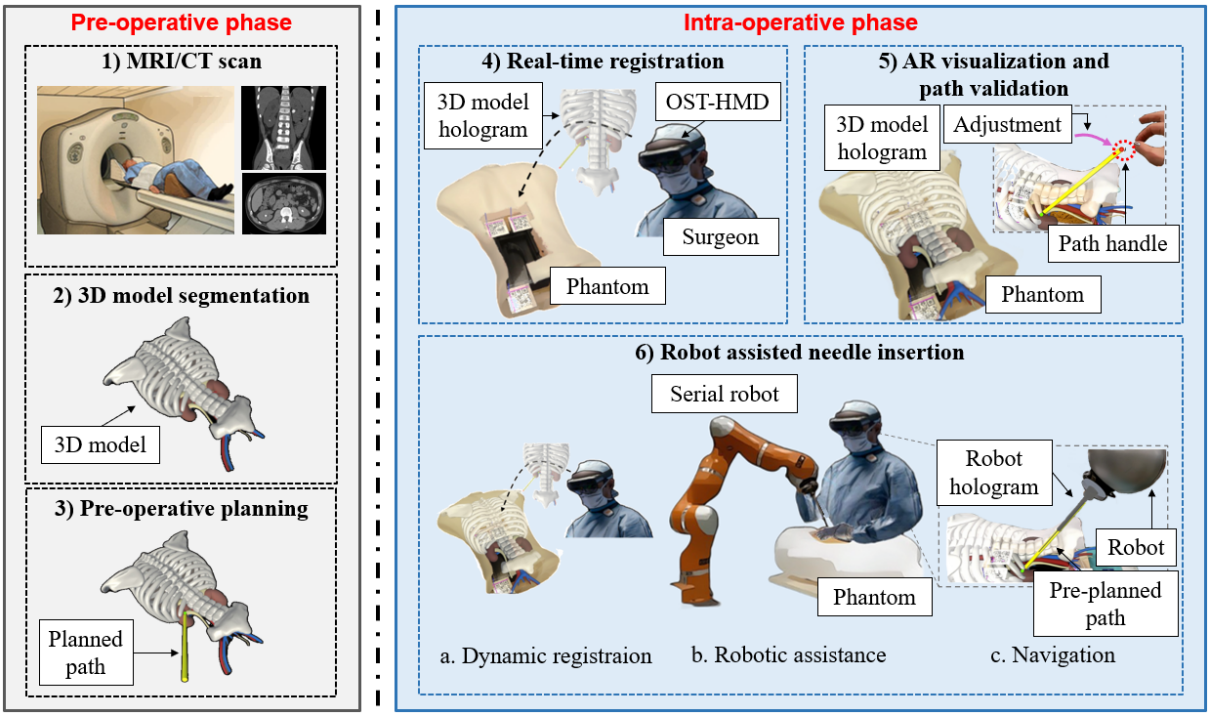

Figure 5: System framework

The system framework consists of two main steps, visualized in Fig 5, the pre-operative phase and the intra-operative phase. In the first one, the patient anatomy is acquired by means of a standard MRI or CT scan Fig 5.1, the structures visualized in the images are then segmented and a 3D model is created Fig 5.2, in the end, the surgeon defines the insertion path onto the 3D model Fig 5.3.
In the intra-operative phase the patient lays in a prone position on the operating bed (Fig 5.4 simulates the real patient position with a phantom). 3 markers are already present on his back since they have been placed before the pre-operative image acquisition, in order to have their location in the 3D model. The 3 markers equipped with QR codes are scanned with the AR glasses, referred as Optical See Through - Head Mounted Display (OST-HMD) in Fig 5, their positions are computed and the AR model is superimposed onto the patient Fig 5.5. At this point the ureter and stone positions are well visualized from the surgeon. The previously defined path position is updated by the surgeon considering also the current positions of the fragile structures to avoid during the maneuver. Once the path is defined, the surgeon freely manipulates the robot to align the tool with the AR visualized path Fig 5.6. At this point the surgeon sends the command to the robot to change the stiffness and allows only the forward movement to perform the insertion without deviating from the path.

This innovative technique was created with the understanding that the surgeon's primary

challenge during kidney puncture is using their imagination to pinpoint the exact position of the organ. Typically, ultrasonography provides horizontal and longitudinal viewing of the kidney as well as information regarding the renal axis, but it only depicts a single-plane image, leaving out key anatomical details like the collecting system. Augmented reality with 3D enhancements can show all pertinent anatomical features at once. There are no shadows from the ribs, which impede vision during ultrasonography and limit the choice of the puncture location. Due to identical positioning and breathing during preoperative CT and intervention, spatial inaccuracies are negligible even if augmented reality wouldn't offer real-time 3D imaging [10].

1 | Literature review

1.1. Robotics in surgery

Due to the many advantages that robotics brings, there are many studies that developed robotic systems for the above-mentioned surgeries. For example in the field of LESS (figure 1.1), which is a minimally invasive surgical technique that is performed through a single incision, typically through the patient's umbilicus, with the advantage of performing the surgery through a single port, resulting in a less noticeable scar. This technique can be used in a variety of surgical procedures, including appendectomies, gallbladder removal, hysterectomies, or prostatectomy.

The study [11] aimed to determine if a LESS procedure, more specifically a single-port transperitoneal robotic-assisted laparoscopic radical prostatectomy (spRALP), is feasible and to discuss its surgical technique.

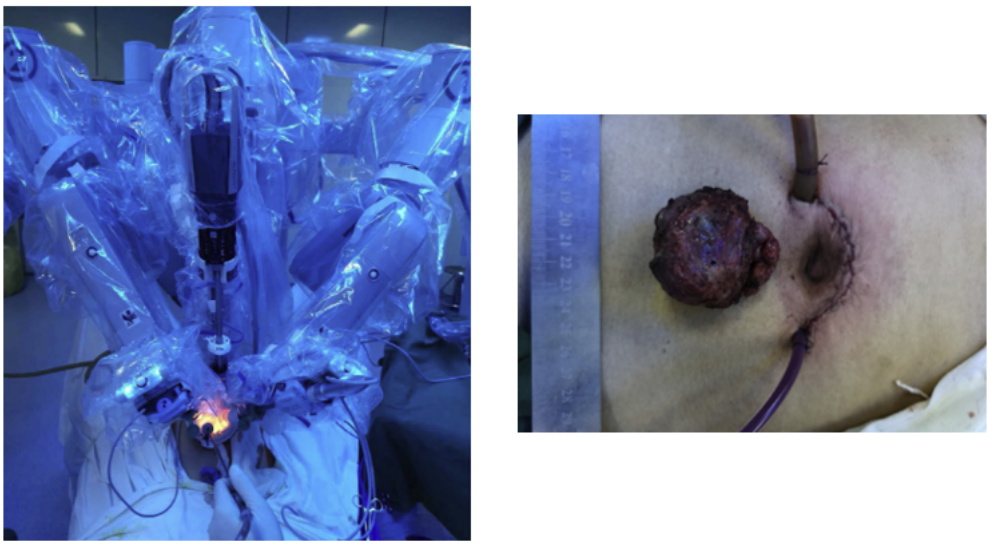

(a) LESS surgery setup (b) LESS reduced wound outcome

Figure 1.1: LESS surgery in prostate tumor resection

The spRALP was performed using the da Vinci Si HD surgical system (figure 1.1) on a patient with prostate cancer. The surgical procedure was consistent with conventional robotic-assisted laparoscopic radical prostatectomy. The surgery was successful, and the patient was discharged on postoperative Day 4. The conclusion was that the use of robotic-assisted surgery provided benefits over traditional laparoscopic surgery, including greater precision and control of surgical instruments, improved visualization, and reduced surgeon fatigue. These advantages may contribute to improved outcomes for patients, such as reduced blood loss and shorter hospital stays. Moreover, concluded that spRALP is feasible in most robotic urological centers, but further studies are required to compare perioperative complications and outcomes with conventional multi-port robotic prostatectomy. Furthermore, there are some limitations associated with this approach. For instance, the small incision port limits the range of movement, while the use of straight robotic arms can result in restricted freedom of movement, leading to a phenomenon known as "chopsticks," whereby instrument cross-over is highly likely, making maneuvering more challenging.

The field of RAS is commonly applied in NOTES procedures, which stands for "Natural Orifice Transluminal Endoscopic Surgery." This surgical technique involves using an endoscope to access and perform surgical procedures through natural orifices in the body, such as the mouth, anus, or vagina and is a minimally invasive approach that eliminates the need for external incisions and reduces the risk of complications associated with traditional open surgery. While NOTES surgeries can be used for various procedures, such as gallbladder removal, appendectomy, and weight loss surgery, this technique is still relatively new, and not all procedures are suitable for it. Moreover, NOTES surgery requires specialized equipment and expertise, and not all hospitals may offer this type of surgery. One typical RAS system used in NOTES is the master and slave transluminal endoscopic robot (MASTER), developed by Nanyang Technological University and National University Health System (refer to Fig. 1.2). The MASTER platform allows for the bimanual steering of two arms, provides dexterity, triangulation, and haptic feedback to maintain spatial orientation, and has a navigation system that allows for real-time maneuvering with the help of three-dimensional reconstruction. The device comprises a master console with a flexible robotic slave, and it incorporates two end effectors, a monopolar electrocautery hook, and a grasper [7].

(a) MASTER's the two robotic arms' end effectors (b) system attached to a conventional endoscope

Figure 1.2: MASTER system

In the study [12], the potential of using the MASTER robot to assist in hepatic resection during NOTES was investigated. The findings revealed that the robot was able to effectively grasp, retract, and excise liver tissue in the desired plane without the need for laparoscopic assistance. The successful performance of hepatic resection on two pigs highlights the potential of the MASTER robot as a promising solution for NOTES procedures. In the end, the study states that the system enhanced precision and dexterity by increasing the degrees of freedom. However, there are some limitations such as the end-effector being larger than the endoscope operative channel making it harder to be used compared to a normal endoscope, and lack of haptic feedback technology.

Moreover, laparoscopic minimally invasive surgery has to be considered. It is a surgical technique that allows surgeons to operate on internal organs and tissues using small incisions instead of large ones. During it, the surgeon makes several small incisions (usually less than 1 cm) in the abdomen and inserts a laparoscope, which is a thin, lighted tube with a camera on the end, through one of the incisions. The camera allows the surgeon to see inside the body on a video monitor. Other instruments are inserted through the other incisions and the surgeon uses them to perform the necessary surgical procedures.
In this application, it is worth mentioning the da Vinci Surgical System (made by Intuitive Surgical, Inc., Sunnyvale, CA; shown) that set the standard for robotic-assisted surgery in 2000 and has since become one of the most frequently utilized robotic surgical systems worldwide. By 2015, there were over 3400 systems in operation globally. The system has been approved for a range of procedures including cardiac, colorectal, general, gynecologic, head and neck, thoracic, and urologic surgery since its introduction [7].
The study [13], aimed to compare the short-term postoperative outcomes of patients who underwent totally minimally invasive radical gastrectomy using the da Vinci Xi robotic system versus manual laparoscopy for gastric adenocarcinoma. Two groups of patients

that underwent surgeries of either one or the other system, were compared in terms of perioperative short-term outcomes.
The study found the operating time in the robotic group was longer than in the laparoscopic group. However, the totally robotic technique with the da Vinci Xi robotic system provides similar short-term results compared to laparoscopic surgery in radical gastrectomy. Overall, the study suggests that the robotic system provides a feasible alternative to laparoscopy for radical gastrectomy.

Figure 1.3: Da Vinci surgical system

The da Vinci surgical robot also allows for performing, anatrophic nephrolithotomy (ANL). Such intervention provides the same treatment as PCNL, but exploits a laparoscopic approach rather than the percutaneous one. As an example, [14] published a study in which three patients with staghorn calculi underwent robot-assisted surgery using the da Vinci system without intra-operative complications. However, the da Vinci robot is not suitable for PCNL which is generally considered a better option for larger kidney stones located in the central or upper part of the kidney, while ANL is a viable option for smaller stones in the lower pole.

Despite the superiority of PCNL in the specific case of big stones, the procedure presents big challenges for the surgeon to get good outcomes. In this context, robotic systems can

be used as skill-trainer devices, directly for supporting the surgeon during insertion or automatically doing it. Many studies have already considered a possible implementation of robotics in the PCNL procedure.
The work of [15], for example, introduced a teleoperated robot framework that can provide training to surgeons as well as assistance during procedures, based on two main components. Firstly, constrained inverse kinematics implements a remote center of motion. This reduces the workload of the procedure by having the surgeon control only the tooltip position rather than the position and the orientation. Secondly, haptic feedback was provided to help guide and teach the surgeon during the procedure. Haptic feedback allows the surgeon to remain in full control during the procedure while still receiving haptic cues and assistance. This system improved accuracy, made the path shorter and smoother, and made procedure time shorter. However, the path planning procedure was still based on intra-operative fluoroscopic images exposing the patient to radiation. Furthermore, the haptic feedback device could be considered less intuitive to a surgeon with respect to a manual procedure with the possibility of impacting the overall efficiency.

The robotic system PAKY (Percutaneous Access to Kidney), firstly introduced in [16] and then improved in [17], included a passive 7-DoF arm holding a radiolucent needle at the end-effector that can be detected in CT images. The robot then, drives its end effector, allowing the needle to move along its axis. The surgeon must manually align the instrument with the desired trajectory before constraining the movement and teleoperating for needle insertion. Despite the alignment of the robot being done by free hand, the needle insertion is still teleoperated and in this work, there is still the presence of fluoroscopic imaging for the navigation alongside the X-rays imaging navigation. The study [5] enhanced the PAKY robotic system by incorporating teleoperated alignment through a joystick, which resulted in the creation of a new system named PAKY-RCM (Remote Center of Motion) (refer to figure 1.4). This new system allowed surgeons to teleoperate the robot during both the alignment and insertion phases while maintaining a fixed RCM, resulting in greater insertion accuracy. However, the use of a joystick control may be less intuitive for surgeons and could lead to a less effective procedure, despite the improved accuracy.

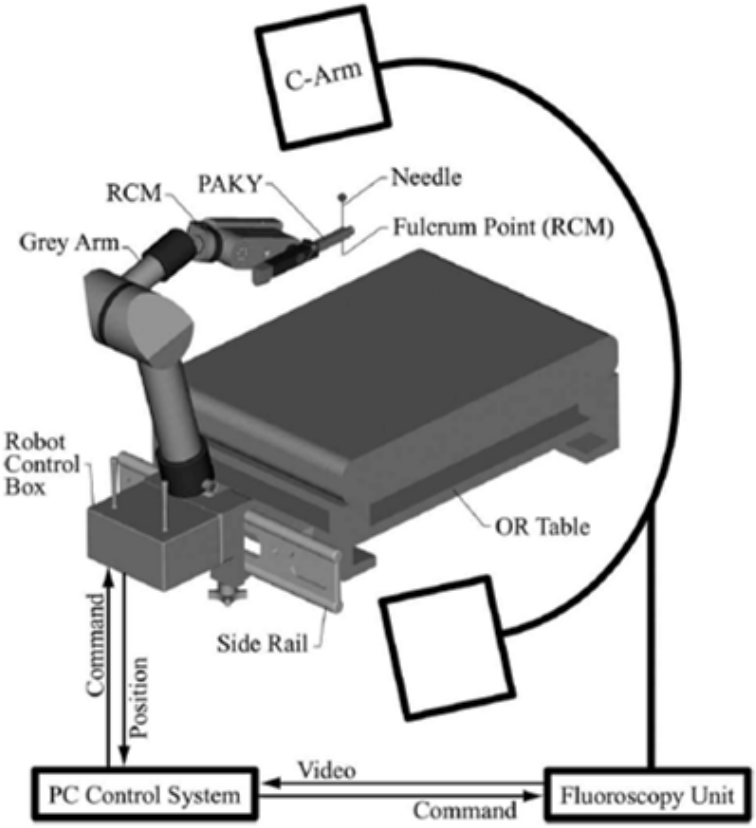

Figure 1.4: PAKY-RCM setup

Reference [2] proposed a three-steps robotic system for percutaneous interventions designed to perform three working stages. The first stage (see figure 1.5.1) involves choosing a suitable percutaneous access point, which is achieved by the surgeon directing the motion of the ultrasound (US) probe with the assistance of the robot. This allows the surgeon to have complete control over the direction of the probe. Then the second stage (see figure 1.5.2) the surgeon releases the probe, and the robot takes over the motion. The robot is programmed to track the respiratory motion of the patient using US image feedback. The third and final stage (see figure 1.5.3) involves the surgeon choosing the moment for the automatic needle insertion. This system improved accuracy, reduced the risk of complications, and improved patient outcomes. Nevertheless, there are some limitations, the total automatic needle insertion procedure makes emergency management more complex and the patient is still exposed to the fluoroscopy radiations.

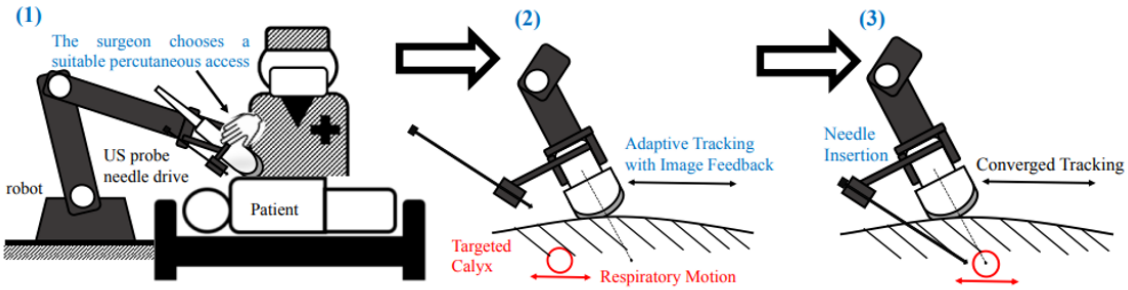

Figure 1.5: Three-steps robotic system schema

1.2. Augmented Reality in surgery

In this section, the second contribution of the current work, hence the Augmented Reality visualization, and its general background literature in surgery is analyzed.

Due to the above-mentioned advantages of AR reality surgery implementation, there are many studies that investigate the possible application of AR in surgery. The study [18] for example, implemented a Microscope-based HUD (Heads-up display), hence a "world device", and discussed the use of AR in lateral skull base surgery, particularly in tumor resection. The conclusion was that the use of AR during the tumor resection helped simulate the procedure and assist in planning the incision and craniotomy. So the AR has the potential to be a useful tool in lateral skull base surgery, but more research is needed to determine its effectiveness and safety. Moreover, the study highlights the potential for distraction and inattentional blindness associated with a crowded field of view and recommends that the minimum amount of critical information expected to create the largest impact be displayed. This enlightens the possible problem of too much added information in the AR environment and consequent operator discomfort.

Another study, [19], proposed a new system that uses display-based augmented reality (see figure 1.6.a) to improve the visualization accuracy of the bowel region and reduce the processing time during surgical procedures. The system places a model developed using CT images of the target object over live video to provide detailed visual output of the target in order to support the surgeon (see figure 1.6.c). Furthermore, the system is capable of running image registration without human involvement and can even decide when to trigger the reregistration process whenever required. Despite the promising results the study proposed only a preliminary analysis with a small sample size, with the evaluation of only the intra-operative phase and not the post-operative phase and, in the end, it runs

the automatic dynamic registration with 30 to 45 frames per second, which is too low for many surgeries.

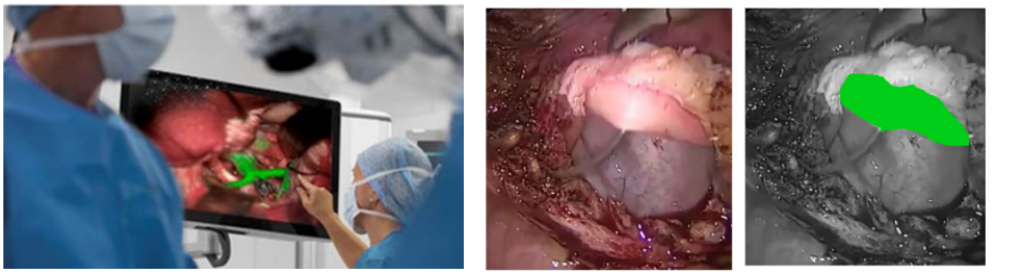

(a) Desktop based AR guided surgery (b) Original image (c) Final image with AR model

Figure 1.6: Display-Base AR target visualization system

The study [20], highlighted the use of a C-arm fluoroscopy system with an augmented reality HMD device (HoloLens2) in orthopedic surgery to provide 3D real-time guidance for surgical procedures, bringing benefits over the traditional 2D visualization of the X-rays. The system was put to the test on a semi-anthropomorphic phantom, and it was shown to be just as accurate as conventional image-guided methods while taking up less time and fewer X-ray images. The authors propose that more investigation is required to examine the potential of this augmented reality support system in more extensive trials focused on typical orthopedic treatments.

The therapeutic impact and technological viability of an augmented reality laparoscopic navigation (ARLN) system during laparoscopic splenectomy, which involves spleen removal, are assessed in [21]. In the study two patient groups underwent laparoscopic splenectomy, one group had laparoscopic splenectomy procedures performed under ARLN supervision and one underwent the procedure with the standard visualization method. The ARLN guiding consisted in displaying the AR 3D model of the pancreas, spleen, and vascular structure on the screen usually used for the procedure. This helped find the avascular area and arrange the position and direction of the treatment. In comparison to the non-ARLN group, the ARLN group had much less intraoperative blood loss and a greater success rate in performing splenic artery dissection. The ARLN group also experienced much less postoperative hospitalization. The study's findings support the use of ARLN as a practical and reliable intraoperative image guidance system during laparoscopic splenectomy for severe splenomegaly.
An AR-based guidance system for hip resurfacing surgery was suggested by the study [22]. The paper makes the case that accurate implant placement is essential for successful hip resurfacing, but that the intrusiveness, expense, and complexity of current

computer-assisted orthopedic surgery systems limit their use.

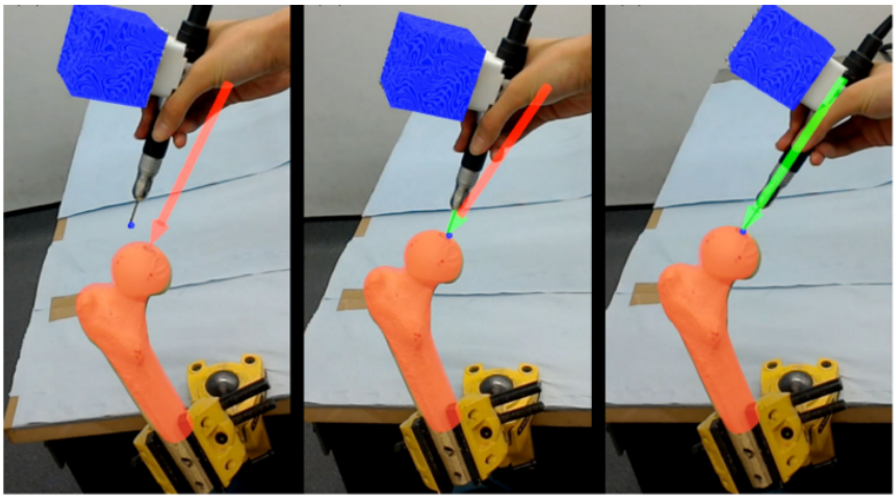

(a) Wrong position and orientation (b) Correct position and wrong orientation (c) Correct position and orientation

Figure 1.7: HMD AR placement visual guidance

The authors presented a method that would let a user do surgery without extra physical guidance by providing intra-operative surgical guidance via an augmented reality headset. In figure 1.7 the visual guidance strategy can be seen, where the augmented path changes color according to the successful alignment or not. Using femur phantoms to drill guide holes, the study conducted trials to evaluate the navigation system's accuracy and discovered that the mean errors were typical of current commercial computer-assisted orthopedic systems. Despite the good indications given by the results, some limitations have to be noticed, in particular the highly artificial setup, in which the femur is completely separated from the rest of the surgical scene, this may lead to increased complexity during a real surgical scenario. In particular, the point cloud registration performed over the femur would be the biggest obstacle to eventual clinical deployment, because the use of machine learning techniques to segment the target femur from the surgical scene may be required.

In order to accurately implant pedicle screws during spine surgery, [23] tested the accuracy of holographic navigation employing a head-mounted device and 3D intraoperative fluoroscopy. The pedicle screw insertion guidance strategy was based on displaying the 3D preoperative planning, by superimposing the real anatomy with a hologram. In an experimental cadaver study, the researchers compared the precision of this method to cutting-edge pose-tracking technology. They came to the conclusion that holographic

navigation using a head-mounted device could reach precision comparable to top-of-the-line pose-tracking systems because they discovered no big differences in accuracy between the two techniques. The work raises the possibility that this methodology could offer a novel method of surgical guidance with minimum infrastructure requirements.

The paper [24] discussed a study comparing fluoroscopy-guided needle placement in a phantom to the accuracy and efficacy of needle placement utilizing an AR navigation platform deployed on a smartphone or HMD devices. The AR reality navigation consisted of the visualization of a virtual path, the target, and the entry point (see figure 1.8). In the trial, six interventional radiologists used cell phones or HMDs guidance to carry out some needle placement procedures. Statistics were recorded for the placement error, placement time, radiation dose-area product, and fluoroscopy time. The findings revealed that whether utilizing smartphones or HMD, the positioning inaccuracy was comparable. However, the smartphone and smartglasses shortened the placement period compared to the fluoroscopy-guided technique. For augmented reality, no intra-procedural radiation was necessary. So, the study came to the conclusion that augmented reality on smartphones and smartglasses decreased needle placement time and radiation exposure while retaining placement accuracy in comparison to a clinically validated method.

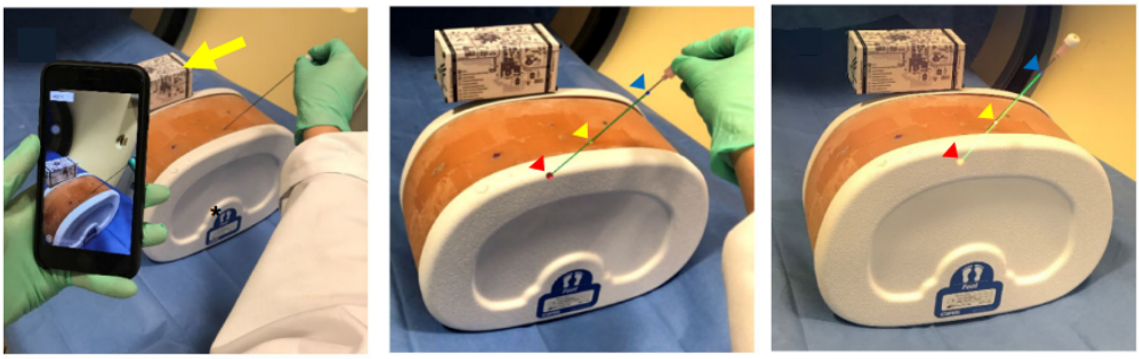

(a) Smartphone Augmented Reality visualization setup

(b) Insertion path visualization

(c) Insertion path validation

Figure 1.8: HMD AR placement visual guidance

Also, this study states some limits, for example, the system has to be used in conjunction with CBCT-guided fluoroscopy to implement effective navigation. Moreover, some operators reported symptoms of cybersickness which is commonly associated with immersive technology.

The first in vivo investigation of an AR system for the direction of percutaneous interventional cancer operations is reported in [25]. The Endosight HMD system was used to

perform percutaneous thermal ablations on patients with liver tumors who participated in the trial. The process entails segmenting the tumor prior to surgery and reconstructing it in three dimensions using CT scans. The probe's target trajectory was then established. By using AR navigation, the procedures were completely directed by AR. The system precision, setup time, and targeting time were the main endpoints. The study discovered that AR guidance is extremely accurate, enabling the operator to confidently perform percutaneous thermal ablations without experiencing any difficulties during or after the procedure or operator cybersickness. The limitations mentioned in the paper include the long learning curve for the use of these technologies, poor working ergonomics, and the difficulty of mental registration of the target position.

Applications of AR in PCNL are already considered, such as in [26]. The purpose of this study was to develop a three-dimensional visualization model of the patient, use it to direct intraoperative puncture in an AR environment and assess the clinical utility and accuracy of the model. The technology uses a three-dimensional model that is visually registered with the patient's body and projected through HoloLens to directly reach the target in the renal calyx. Routine percutaneous nephrolithotomy was performed on a control group under B-ultrasound supervision. According to the study, the group using AR performed better than the control group in terms of stone clearance rate and postoperative complications due to shorter puncture times, fewer puncture attempts, and shorter puncture times overall. The AR application in PCNL demonstrated acceptable accuracy and good value for guiding puncture in a mixed reality setting, according to the authors' findings. However, just like many other studies already considered, the navigation system needs X-rays hence the patient and personnel irradiation.

1.3. State of the art in PCNL

By looking at the above literature review, it can be seen that both robotics and AR are spreading in surgery thanks to their ability to reduce some limitations of the current surgery setups. In particular, from the above sections, it can be inferred that the two technologies bring different contributions to the field. Robotics' main contribution is to increase surgeons' physical capabilities from an accuracy, dexterity, and task repeatability point of view. AR main contribution instead, increases the surgeon's perception, by enhancing context awareness and making the surgeon make better decisions.
Furthermore, in the above literature review sections, it has been seen that both AR and Robotics have already been employed in PCNL in order to reduce the high surgeon workload and the high accuracy in the needle insertion demand.

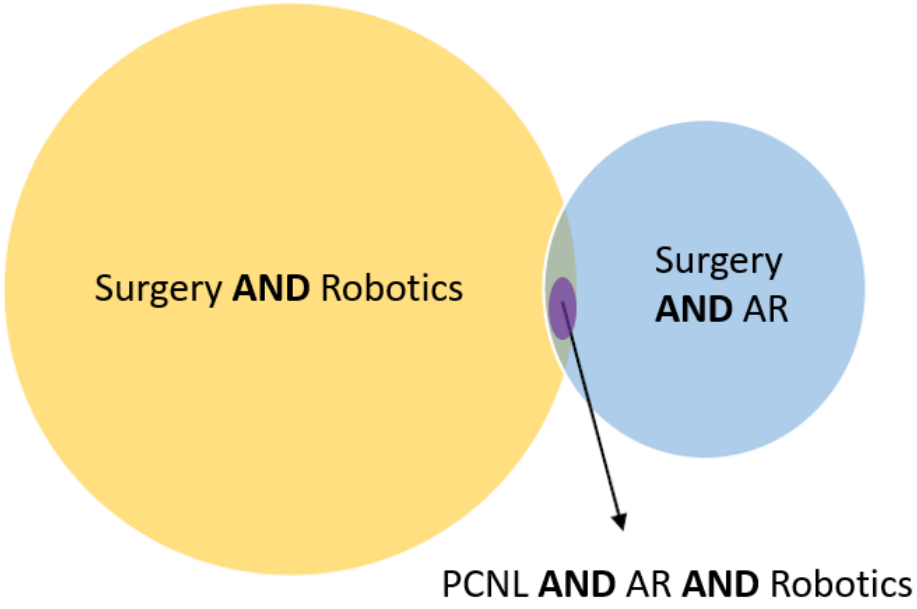

Figure 1.9: Work research division

The aim of the following section will be to understand whether the two systems can work together in the PCNL procedure, or more in general into needle insertion tasks, and sum up the positive contributions they bring individually or whether their coexistence would be contraindicative. In order to understand it, this section reviews the top research on cutting-edge technologies that combined robotics and AR visualization and can be used PCNL needle insertion procedure. (figure 1.9).

As already mentioned in the section 1.1, robotics started being used in surgery in the 1980s, the earliest application of robotics to urologic surgery, though, began in 1989 demonstrating the ability of robots to perform a precise, repetitive, and controlled tasks in accomplishing transurethral resection of the prostate [5].

For what concerns the AR visualization in the context of PCNL surgery instead, the visualization of the renal anatomy has been proven to be sufficient for estimating the correct needle angles to reach the target [27]. Such visualization is enabled by the proper tracking and registration of the internal conditions of the anatomical structures of the patient reconstructed intraoperatively by means of ultrasound images.

There are studies that implement both AR visualization and robotic assistance into PCNL. The study [4] for example, proposed this type of combined innovative approach. This

system can assist both expert and novice surgeons in improving the performance of surgical operations. The paper validates the proposed system on a setup including a KUKA LWR 4+ robot and the Microsoft HoloLens as an AR headset. The AR system is designed in order to implement the visualization of the patient's anatomy, alongside the target stone and insertion path (see figure 1.10.a). The Robotic assistance system instead implements a system of virtual fixtures to support the surgeon during the alignment and the insertion of the robot (see figure 1.10.b).

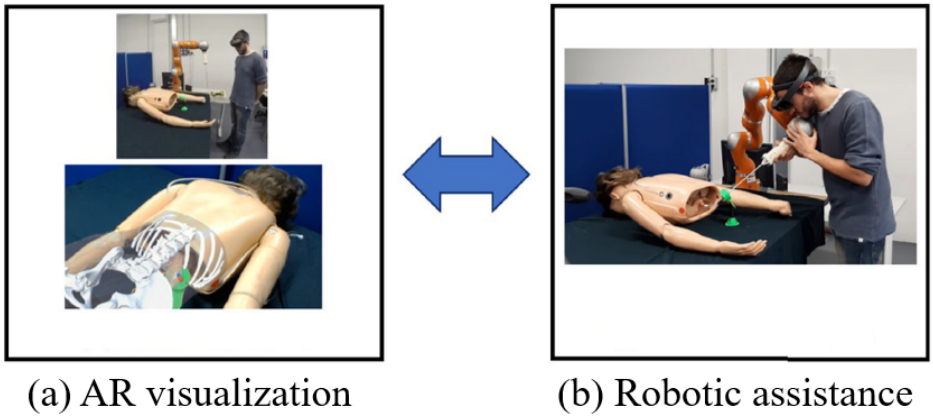

Figure 1.10: Proposed AR and Robot-assisted combined approach

The study runs some user studies to evaluate the system from both the accuracy and usability points of view. Despite implementing both an AR visualization and robotic assistance, the user tests are performed only over the robotic assistance system, by always implementing AR. This method of validation can only give an accurate point of view over the virtual fixtures system while it gives only a general point of view, with general accuracy values for the AR visualization system. In any case, the study states a positive contribution of the virtual fixtures when performing the procedure and that the virtual fixtures return a positive contribution in terms of usability of the system and not only from the performance point of view, if compared to the application of a sole AR support. Other limitations of the work can be found in the absence of AR navigation, the system in fact, despite using robotic assistance, doesn't visualize a holographic couple of the robot bringing the need for fluoroscopy navigation to perceive the position of the robot once inserted in the patient.

[28] is another study that is worth mentioning for the design of AR and robotic-assisted systems for needle insertion procedures. This study implements the system into orthopedic surgery, more specifically in the pedicle screw placement, but with the possibility to adapt the system to any needle insertion procedure, such as the PCNL one. The paper

argues that current robotic systems cannot rely solely on preoperative planning and require extra adjustments to adapt to intraoperative changes. The proposed system uses a head-mounted display (HMD) and AR to offer an intuitive display of the surgical site and anatomy, allowing surgeons to fine-tune the surgical plan and transfer it immediately to the robot for execution. The system framework consisted of the possibility of the user aligning an AR arrow with the desired insertion path as assessed by the user himself based on the AR information about the anatomy structure. Once the AR arrow was considered in place, it was possible to press an AR GUI button to perform the totally automatic robot alignment and needle insertion. The paper demonstrates the technical feasibility of the proposed system through a series of experiments, evaluating system accuracy and human-related errors. The proposed AR-based robotic approach could facilitate robotic technology in the operating room and boost synergy between AR and robots for other medical applications. The authors of this system have acknowledged its limitations, particularly in the robot registration procedure. While the procedure does not rely on any external tracker that would increase system complexity, it does result in lower registration accuracy. Another limitation is the path instability due to the HoloLens hand recognition feature that is still active during the alignment, causing the HoloLens to interpret the path as grabbed and moved.

By looking at the current state of the art it can be seen that currently existing AR-based navigation systems have not been fully integrated with robotic-assisted systems despite the promising premises.
A different potential article, [29], describes a study intended to increase the precision and safety of cervical pedicle screw (CPS) placement surgery using a combination of real-time soft tissue deformation tracking with relative AR visualization, and hand tremble compensation, integrated into a surgical robotic system (figure 1.11). Based on previous shape models and intraoperative ultrasound pictures, the paper suggests a method for computing soft tissue deformation and updates the structure representation of the deformed target tissue accordingly. The robotic aid took the form of a straightforward mechanism for compensating for hand tremors, which increased the resilience and precision of the virtual-physical calibration process. The outcomes of phantom and animal studies show that the suggested system is workable and precise.

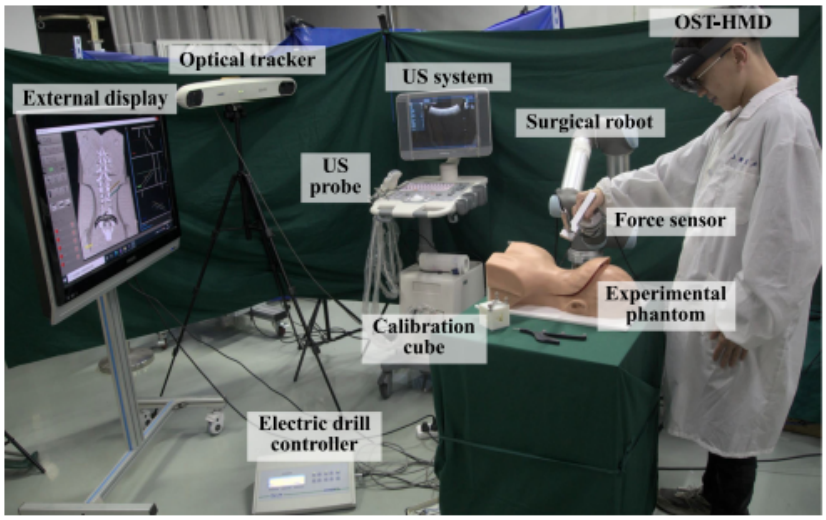

Figure 1.11: Real-time soft tissue deformation AR visualization and hand tremble compensation system setup

According to the paper's findings, the proposed technology has substantial clinical application potential and can improve the efficiency and safety of CPS placement surgery. However, this system implements a simple hand tremor reduction system, not a full procedure robotic assistance, further improvement could be implemented.

1.4. Motivation and objectives

After stating the PCNL needle insertion procedure challenges and limitations, alongside the current state of the art in the robotic-assisted and AR visualization of needle insertion the following work objective has been defined.
The objective of the work is built on the above considerations, by trying to take the best advantages of all the systems considered above and to reduce the limitations.
It has been seen that most of the studies that consider the implementation of robotic-assisted needle insertion, either implement a totally automatic procedure that doesn't give freedom of correction over the stages of the surgery to the doctor, or they implement a teleoperation control that can be counterintuitive and reduce the surgery outcome. In all the cases of robotic systems, the radiation exposure was not reduced. AR systems instead, although all of them were improving the surgeon perception, some of them were still implementing the fluoroscopy for the navigation, and some others were not considered valuable strategies to reduce the hologram drift. The hologram drift is a typical problem of AR in which the virtual object moves away from where it was originally placed, for this reason, the surgeon could need to re-calibrate the system during the procedure,

which could reduce the surgery outcome quality. Therefore, the two technologies can be implemented to reach different aims and also different problems present in the gray literature:

AR visualization:

- Radiation exposure reduction: The AR visualization system, as it can be inferred from the above literature review, can be implemented to substitute the standard X-rays imaging techniques to visualize the target location and reduce personnel and patient radiation exposure.
- Context awareness enhancement: The use of AR technology allows surgeons to visualize the patient's anatomy in 3D and with a see-through feature, providing an enhanced perception of the context. This means that virtual objects can be seen where they actually are, regardless of any obstacles that may block direct visualization.
- Intra-operative path validation: The use of AR visualization results in improved context awareness, allowing for a greater perception of the positions of fragile structures within the patient. This enhanced awareness enables the system to validate pre-planned paths that were built over pre-operative images displayed on a 2D screen, providing the advantages of 3D perception during the planning procedure.
- Dynamic registration: This is a feature that can be implemented to reduce the hologram drift problem mentioned above, which is a limitation of the AR devices, not the surgery itself, but that is not addressed by many studies.
- Robot calibration: The aim will be to improve the holographic robot and real robot overlapping inside the AR environment. This problem has not been addressed or has been addressed with bad results, with many studies in the needle insertion field because they were not visualizing the robot hologram or they implemented registration strategies without the implementation of external tracking systems.

Robotic assistance:

- Alignment accuracy enhancement: Thanks to the robot assistance and the shared control between the human operator and the robot, it is possible to make fine movements and precisely align with a pre-planned path. The result, as has been seen in the above considerations, is a more precise alignment with the pre-planned path and a more controlled movement along it.
- Procedure repeatability enhancement: is introduced because robots can perform the same task over and over again with the same level of accuracy and precision. This

is due to the fact that robots are programmed to follow a specific set of instructions, which they execute with consistency and accuracy. Unlike humans, robots do not get tired or lose concentration, and they can perform the same task repeatedly without making mistakes.

- Hand tremor reduction: Robots are inherently stable due to their design, which means that they can remain steady and maintain a fixed position while performing a task. This stability can be particularly useful when working with small or fragile objects that require a steady hand, as the robot can provide a stable platform for the human to work on. Furthermore, hand tremors can be exacerbated by fatigue, stress, or other factors that can affect the human operator. Using a robot assistant can help reduce their overall workload and minimize the risk of fatigue.

By implementing both technologies in the system the following main objectives can be defined.

Combined systems:

- Effective procedure navigation: The combination of both AR and Robotic assistance can implement an AR navigation system without the need for external tracking devices or X-rays. The current robot's position in space, in fact, can be retrieved directly from the robot joint states. The position than can be sent to the AR HMD creating an effective 3D real-time navigation system.

- Insertion accuracy enhancement: The expected outcome of the integration of the two systems is the increase in accuracy, not only for the reason stated in the Robotic assistance section above but also thanks to the AR visualization of the target combined with the just mentioned navigation system.

- Surgeon workload reduction: The PCNL procedure, as stated in the introduction, is very demanding for the surgeon that needs to identify the ureter position by means of the fluoroscopy images, identify the soft tissues with the US probe, interact with the nurses and perform a precise needle insertion. The implementation of a more intuitive 3D visualization method as the AR one is, and introducing the robotic assistance making a more precise insertion in an easier way, can reduce the overall workload.

2 | Materials and methods

This chapter is focused on the description of the instrumentation and the methodologies used to carry out this study, including also the packages and libraries used during the process. This project was developed both on Windows 10 operating system for the Augmented Reality part and Ubuntu system for the Robotic part.

2.1. System Design and Implementation

In order to achieve the implementation of the system different devices, tools and programs have to be employed, this creates the need for an effective communication network that lets the different modules exchange data.

2.1.1. Overview of the system

The devices, tools and programs that have been defined to implement the system, with corresponding usage, are the following ones:

- Hardware:
  - HoloLens2: Optical See Through - Head Mounted Display device (OST-HMD), used to visualize the 3D AR model of the patient superimposed onto the real patient.
  - Kuka LWR-4+: a robotic arm that by implementing an impedance control strategy guides the user in the insertion procedure.
  - Polaris Vicra NDI: Optical Tracking device (OT) used to acquire the phantom and robot position in space and perform the system calibration.
- Software:
  - Unity: game engine running on Windows 10, used to create 3D and 2D games widely adopted by industries also outside video gaming, such as film, automotive, architecture, engineering, and construction. Used in the current work to

develop the AR interface to deploy in the HoloLens2.

- MRTK: Mixed-Reality Toolkit for Unity, a Microsoft-driven project that provides a set of components and features, used to accelerate cross-platform Augmented Reality app development in Unity.
- ROS: Robot Operating System open-source framework running on Ubuntu system, used for the Kuka LWR 4 robot control.
- Matlab: a programming language and numeric computing environment that allows matrix manipulations, plotting of functions and data, and implementation of algorithms. The current work is running on Windows environment to make some accuracy evaluation measurements and system calibration.

2.1.2. HoloLens - Robot connection

The HoloLens to Robot connection is necessary for two reasons: i) control of the robot with the graphic interface running in the HoloLens; ii) visualization of the holographic twin of the real robot in the AR world. The HoloLens-Robot connection is performed by passing by the ROS network, as it can be seen in Fig. 2.1, the Robot is connected to the ROS environment PC and to the ROS network by means of an ethernet cable. The HoloLens connect to the ROS network by means of TCP-IP over the Wi-Fi network, in order to let the user have free movement.

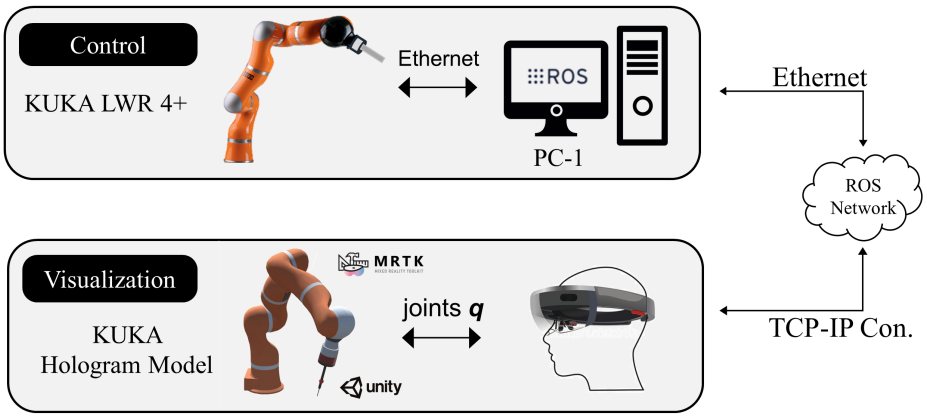

Figure 2.1: HoloLens - Robot connection schema

The Unity package to import in both the application and the ROS workspace in order to create the connection is the "ROS TCP connector". This package provides a set of scripts and files to create the server and clients over the network and to define the message

structures that the two sides are going to exchange. In particular for this application, on the ROS side, at the start-up of the system, a server node is created that can accept all the requests for connection from the clients on the network. The HoloLens app, when turned on, will automatically search for the server with the specified IP and will establish a connection. Once the connection is established the exchange of 2 types of messages is allowed: the "/Stiffness" message and the "/JointsState" message.
The two messages have two very different structures:

- /Stiffness message contains 7 double type variables: $k_x, k_y, k_z, k_{rx}, k_{ry}, k_{rz}, a$ that represent the values of the stiffness constant for the position (k_x, k_y, k_z) and for the orientation (k_{rx}, k_{ry}, k_{rz}) plus the variable a that is sent from unity to ROS to indicate whether the robot is aligned $(a = 1)$ or not $(a = 0)$. For more details about the impedance controller formulas and functioning see section 2.3.
- /JointsState message contains 7 double type variables: $a1, a2, a3, a4, a5, a6, e1$ representing the joint parameters of the 7 rotational joints of the KUKA robot. So all 7 parameters represent the rotation angle of the joint in radiants.

The /Stiffness message is sent from unity to ROS at every iteration of unity, so at a frequency of 60Hz. When the user considers to be aligned, he will press the button and the /Stiffness message will change value. On the ROS side, there will be running a Stiffness_subscriber script that associates the /Stiffness message to the ROS topic /lwr/cartesian_impedence_controller/command, causing the following change of stiffness of the real Robot. In order to achieve the predefined result the following /Stiffness messages have been designed:

Robot not aligned:

$$k_x = 50, k_y = 50, k_z = 50, k_{rx} = 10, k_{ry} = 10, k_{rz} = 10, a = 0 \tag{2.1}$$

Robot aligned:

$$k_x = 3000, k_y = 3000, k_z = 1, k_{rx} = 200, k_{ry} = 200, k_{rz} = 200, a = 1 \tag{2.2}$$

The /JointsStates variable is sent from ROS to the HoloLens by means of a Joints_publisher node that sends the ROS topic /JointsStates to the HoloLens over the TCPconnection. On the HoloLens side there is a script reading the message every time it is published and associates the joints values to the KUKA holographic model joints.

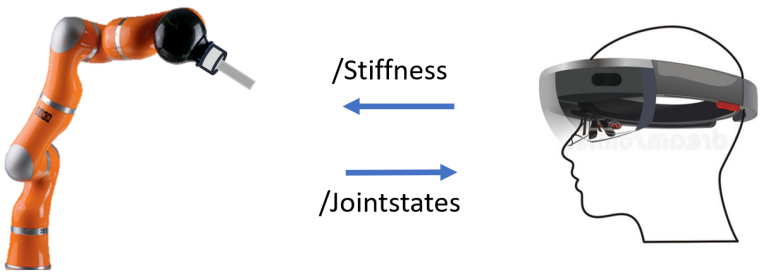

Figure 2.2: HoloLens-ROS message exchange

2.1.3. HoloLens – Matlab connection

The HoloLens to Matlab connection is necessary for two reasons: i) sending the calibration resulting transform from Matlab to the glasses, in the way to overlay the holographic robot in the AR world onto the real one, and ii) sending the resulting transformation of the phantom model registration computed in the HoloLens (see section 2.2.1) to Matlab for the accuracy evaluation. The connection is performed using the Instrument Control Matlab Toolbox which gives the tools to create a TCP/IP connection. The communication is created by running a script in Matlab that launches a server over the Windows machine IP and that accepts all the client's connection requests. The HoloLens request to connect is sent every time the user wants to send or receive a message by pressing the corresponding button in the AR Graphic User Interface (GUI). The connection is again made over the Wi-Fi.

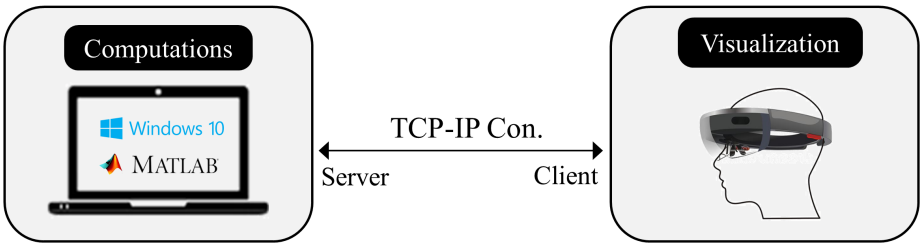

Figure 2.3: HoloLens-Matlab connection schema

Connection workflows:

- Robot registration result: sent from Matlab to the HoloLens, once the calibration between the Optical Tracker, the Robot, and the Phantom has been performed (see section 2.2.2) and consequently the transformation matrix T_{Ph}^{R} has been computed. The Matlab script creates the server over the Wi-Fi networks and waits for a client

request for connection. When the user presses the "Receive calibration" GUI button, the associated HoloLens script connects to the server. Once the connection is detected from Matlab the T_{Ph}^{R} matrix, is sent over the connection as a sequence of char variables coded into ASCII. The received sequence of bytes is then converted back to double type variables and the transformation is applied to the Holographic couple of the KUKA.

- Phantom registration result: sent from HoloLens to Matlab, once the phantom registration has been performed (see section 2.2.1) and consequently the matrix T_{Ho}^{Ph} has been computed. The user has to run the Matlab script to create the server over the TCP/IP connection. When the "Verify registration" GUI button is pressed, the HoloLens connect to the server and send the coded T_{Ho}^{Ph} matrix over the connection. The Matlab script decodes the received matrix and performs the accuracy measurements as stated in the section 2.2.1.

2.1.4. System implementation

In order to implement the system and perform the user test other material with respect to the hardware listed in the section 2.1.1 is needed. In particular, the needed material is a phantom model on which to perform the test and to have a more realistic emulation of the operating room, and an end-effector to equip onto the robot that is suitable for an insertion procedure.

Phantom model The phantom model built for the experimental validation had the following requirements:

- Realistic aspect of the patient body
- Realistic model of the ureter with its 3D digital model for the AR visualization
- Accurate positioning of the ureter with respect to the 3 QR codes used for the phantom registration (Sec. 2.2.1), in the way to have the smallest possible error between the holographic ureter and the real one
- Accurate positioning of 10 fiducial markers needed for the robot registration (see figure 2.16 in sec. 2.2.2)

The strategy to meet these requirements consists of dividing the phantom into 2 parts (Figure 2.4): (i) a 3D printed model furnished with the fiducial markers, the QR codes application sites and the ureter, and (ii) a plastic manikin used to emulate the aspect of the patient body.

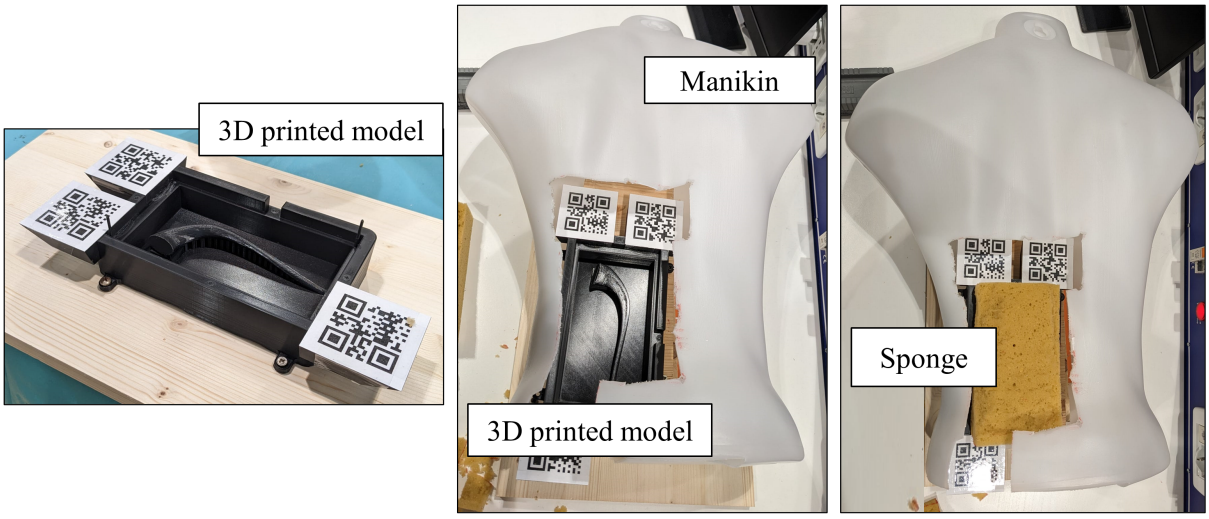

Figure 2.4: Phantom parts: 3D printed box placed into manikin

The advantages of 3D printing (made by using the printer Ultimaker S3) are that it is possible to create a real 3D model of a 3D digital model saved in format STL file. This feature addresses the requirement of having the digital model of the ureter that was needed to be visualized with the AR. Importing the model into the Unity project is, in fact, straightforward since it is enough to convert the STL file into an OBJ one.
Alongside this advantage there is the possibility to have an accurate positioning of the QR code application sites and the fiducial markers, addressing also other two requirements listed above.

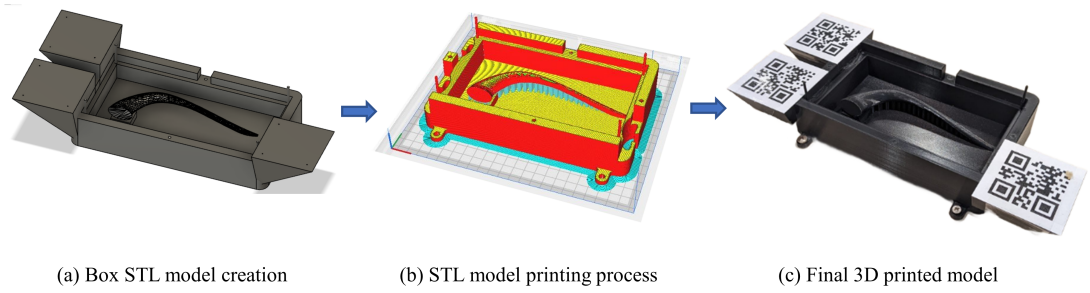

(a) Box STL model creation (b) STL model printing process (c) Final 3D printed model

Figure 2.5: Ureter box creation process

In Figure 2.5 the process of creation of the printed model is shown. In particular in Figure 2.5.a the box design, created with the program Fusion 360, is shown. The design had to take into account three main requirements:

- **QR code size:** The QR code specifications have been designed in accordance with the HoloLens web page guidelines to ensure effective QR code tracking. These guidelines indicate that the minimum QR code size should be 5cm x 5cm with 9mm of white margin for each side. Seen the limited space on the phantom the QR code sites have been defined to host the smallest possible QR codes.
- **Fiducial markers positioning:** The fiducial markers had to be hollow in order to host the Optical-Tracker probe without making it move too easily, a hole of 1mm of depth and 1mm of radius has been chosen to be placed in the position of the fiducial markers. In addition to the size design, the positioning of the fiducial markers was also crucial for the effectiveness of the SVD registration. The markers were placed with a uniform and evenly distributed pattern around the ureter. Moreover, they were positioned in such a way that no plane could contain all of them, which helped to maximize the accuracy of the SVD registration.
- **Ureter size:** The ureter size had to be the one of a real human ureter that on average has 25mm diameter at the calix that goes down to 6mm diameter towards the bladder with an overall length of 20cm.

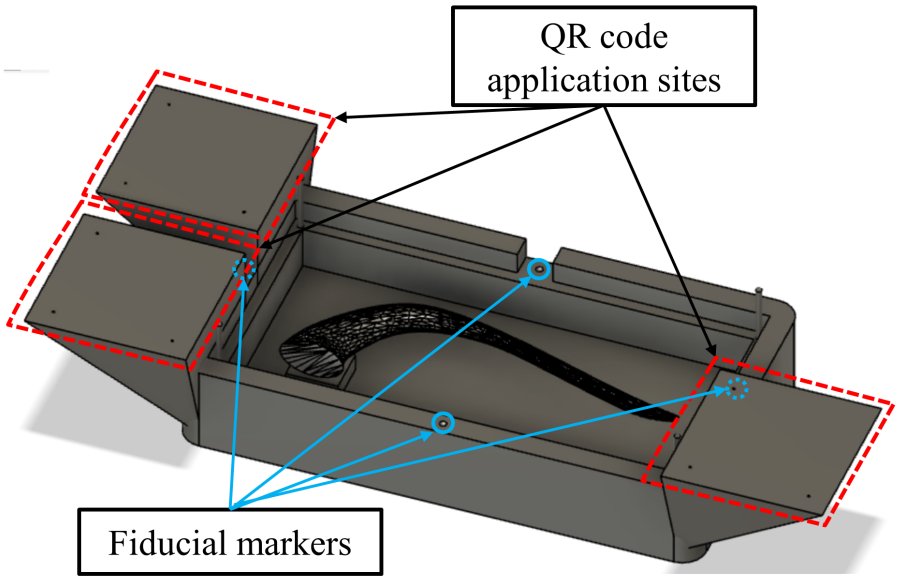

Figure 2.6: Ureter box design

At the end of the phantom creation process, a sponge was placed on top of the ureter box to occlude the view of the ureter from the operator while still allowing for the insertion procedure to take place (see Figure 2.4).

Needle In order to perform the insertion procedure a sharp and long enough needle had to be equipped onto the KUKA robot. The tool chosen for the PCNL procedure is depicted in Figure 2.7.a, which has a needle length of 10 cm and an overall length of 25 cm. This length provides ample space for the operator to grasp and manipulate the tool during the procedure.
To enable visualization of the tool on the holographic twin of the robot in the augmented reality environment, a digital version of the tool was created using the Fusion 360 software (as shown in Figure 2.7.a). The digital model was then exported in the OBJ file format, which allowed it to be imported into the Unity world.

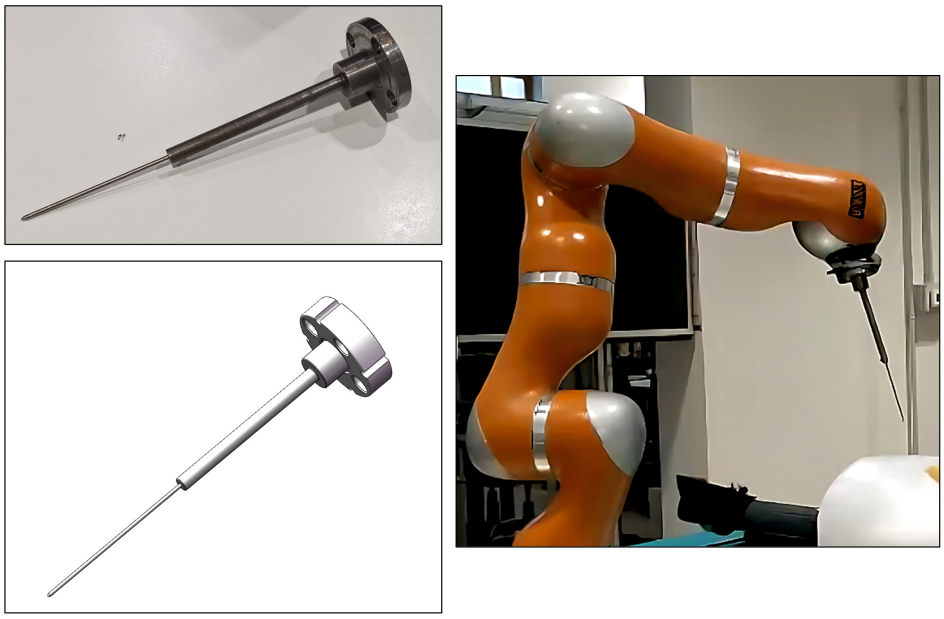

(a) Real needle and its digital model (b) Needle application onto the robot

Figure 2.7: Needle design and equipment

Needle calibration Once the tool had been equipped on the robot, see Figure 2.7.b, it had to be calibrated. The calibration process is fundamental for two main reasons: (i) inputting the tool weight and center of mass location in order to let the robot compensate for its load and (ii) inputting the needle tip position with respect to the RF_{EE} in order to acquire the position of the tip during the insertion and perform the accuracy evaluation.

i. The tool has a weight of 36.4g measured with the scale and a center of mass position equal to (0,0, 3cm), with respect to RF_{EE}, found empirically by running the gravity compensation on the robot and verifying the correct load compensation.

ii. The tooltip position is instead calibrated by means of the "4-points TCP (Tool Center Point) calibration" [30] already furnished by the KUKA robot. This method

gives a much higher accuracy positioning of the tooltip compared to the manual tool length input. The procedure functioning is described below:

In order to perform a TCP calibration of the tool attached to the robot's end effector, the robot is manually moved from the operator to a series of predetermined positions (points P1, P2, P3 and P4 of Figure 2.8) while keeping the tooltip fixed into a specific point (the TCP point in 2.8). The fixed point is indicated to the operator by means of a Calibration Object (Figure 2.8) in order to have a reference where to place the tooltip.
This procedure builds a system of equations that have as an unknown variable the TCP position and as known parameters the positions P1, P2, P3 and P4, determined automatically from the KUKA robot with the forward kinematics.
The final result of the whole procedure is a mathematical system of 4 equations, one for each point P that then is solved to obtain the point TCP, hence the tooltip position in the RF_{EE}.

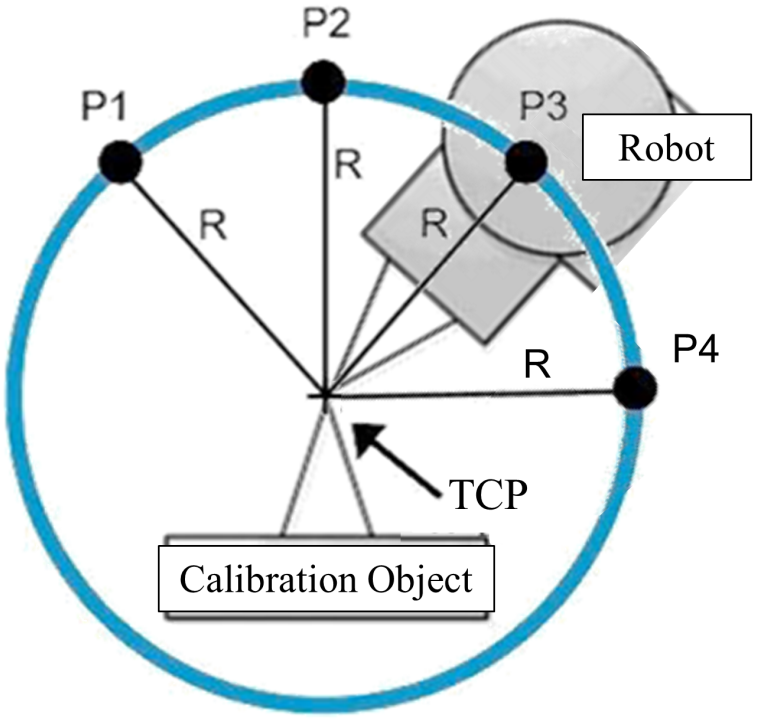

Figure 2.8: TCP procedure general schema

2.2. Registration

The registration procedure is fundamental to compute the coordinates transformations between the Reference Frames of the HoloLens (RF_{Ho}), the robot (RF_R) and the phantom (RF_{Ph}). These three reference frames are defined in different ways. The RF_{Ho} is built automatically from the HoloLens at the start-up of the application and corresponds to the pose of the glasses in the world when the application is loaded, when the user with the glasses will move in the world, the HoloLens RF will be still and the pose of the glasses in the RF_{Ho} will be updated. The RF_{Ph} is built by defining 3 points, corresponding to the position of 3 QR codes, that then are treated as in section 2.2.1. In the end, the robot RF corresponds to the robot base RF as defined in the KUKA manual. The reference frames system can be seen in Figure 2.9

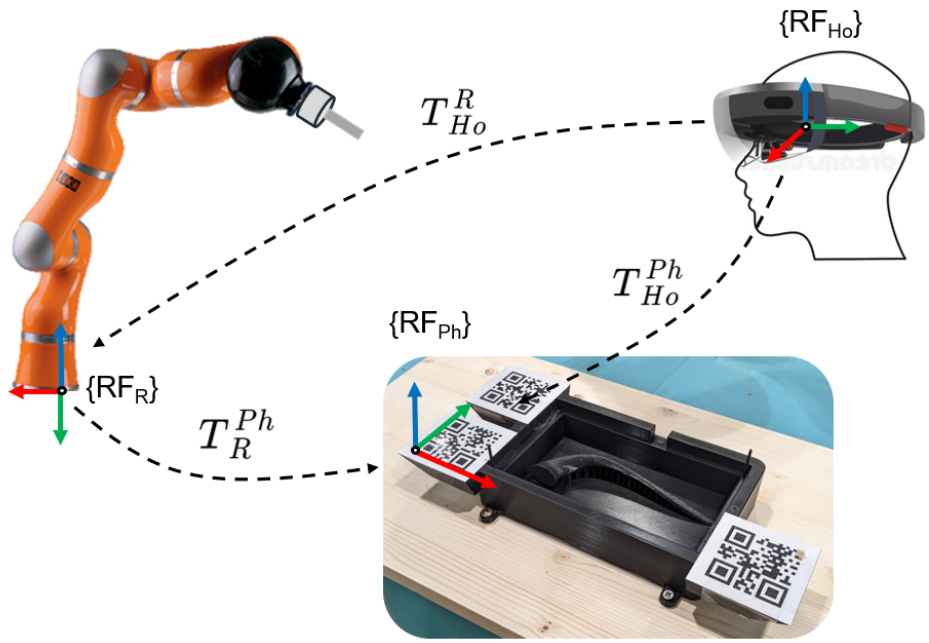

Figure 2.9: System's reference frames

The T_{Ho}^{Ph} transformation is needed to let the user visualize the patient 3D model overlaid on the real patient or the phantom as in the experimental validation case. The T_{Ho}^{R} transformation is needed to visualize the Holographic twin of the robot overlaid onto the real one, in order to implement the navigation system. To measure these two transformation matrices two different registration methods have been employed, one that computes T_{Ho}^{Ph}, called phantom registration, and one that computes the transformation T_{R}^{Ph}, called robot registration, so that T_{Ho}^{R} can be computed with the chain rule as $T_{Ho}^{R} = T_{Ho}^{Ph} \cdot T_{R}^{Ph-1}$.

2.2.1. Phantom registration

The phantom registration method, as mentioned above, is used to compute the T_{Ho}^{Ph} transformation matrix. In order to do so, 3 QR code markers have been applied onto the phantom model, with a know position with respect to the ureter and the other anatomical structures. The QR code scanning feature of the HoloLens is then used to acquire the QR code positions in the HoloLens coordinate system and the 3 positions are used to build the phantom RF.

Phantom RF building procedure: the three QR codes positions are saved depending on the specific QR code, the one that codifies a "1" is saved as the RF origin O, and the ones that codify a "2" and a "3" are respectively saved in $P2$ and $P3$ to define the RF's y and x axis as shown in the Figure 2.10. To build the phantom RF the following computations are performed in a script running in the HoloLens:

$$\begin{aligned} \tilde{x} &= P3 - O,\ x = \frac{\tilde{x}}{\| \tilde{x} \|} \text{ , x axis direction definition and normalization} \\ \tilde{y} &= P2 - O,\ y = \frac{\tilde{y}}{\| \tilde{y} \|} \text{ , y axis direction definition and normalization} \\ z &= x \times y \text{ , computation of the z axis as the cross product of x and y} \end{aligned} \tag{2.3}$$

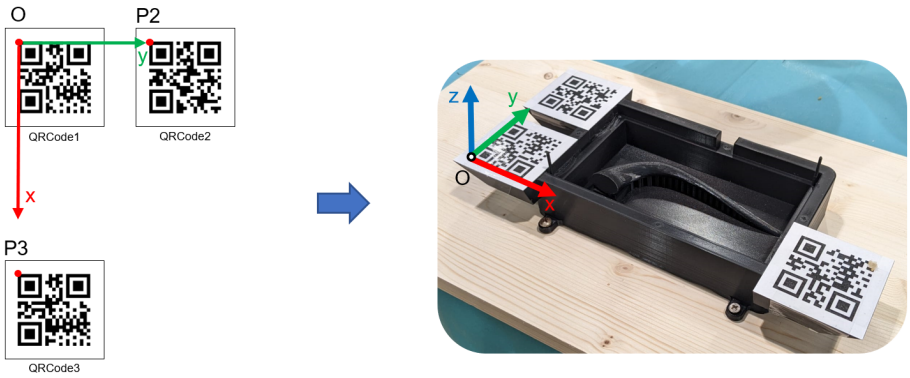

Figure 2.10: Phantom RF building procedure

Holographic model registration: Once the phantom RF has been defined, it can be used to perform the registration. Hence to compute the transformation matrix between the HoloLens RF and the phantom RF. In order to do so, a paired point registration method is applied between the two sets of points:

- $\{O,\ P2,\ P3\}$ points of the RF_{PH} acquired in the section above
- $\{O_{Ho},\ X_{Ho},\ Z_{Ho}\}$ defined as $O_{Ho} = (0,0,0)$, $X_{Ho} = (1,0,0)$ and ${}_{Ho}Z = (0,0,1)$ in the RF_{Ho}

An observation to make is that the third point pair of the two sets is between $P3$ and Z_{Ho}, so between the y axis of the RF_{PH} and the z axis of the RF_{Ho}, this happens because the HoloLens coordinate system is Left-Handed while the Phantom coordinate system is Right-Handed.
After defining the two sets of points, the Unity built-in function Quaternion.LookRotation() is applied to compute the paired point registration. This built-in function takes as input the directions of the two phantom axis x_{Ph} and y_{Ph} and gives as output the RF_{Ph} orientation inside the RF_{Ho} which corresponds to the rotation matrix R_{Ho}^{Ph}. The translation instead is $O_{Ph} - O_{Ho}$ with $O_{Ho} = (0,0,0)$, so the final transformation matrix is:

$$T_{Ho}^{Ph} = \begin{bmatrix} & R_{Ho}^{Ph} & & O_{Ph} \\ 0 & 0 & 0 & 1 \end{bmatrix} \tag{2.4}$$

Registration workflow: In order to perform the RF_{Ph} registration and the T_{Ho}^{Ph} computations as stated above, the user has to press the Scan GUI button, this event makes the HoloLens scan the environment to acquire the specified QR codes positions as shown in Figure 2.11.a. Once the acquisition is performed, the user presses the Stop scan GUI button and the three acquired points are treated as above to compute T_{Ho}^{Ph}, then the transformation matrix is applied to the 3D model of the patient that is visualized overlaid onto the phantom, see Figure 2.11.b.

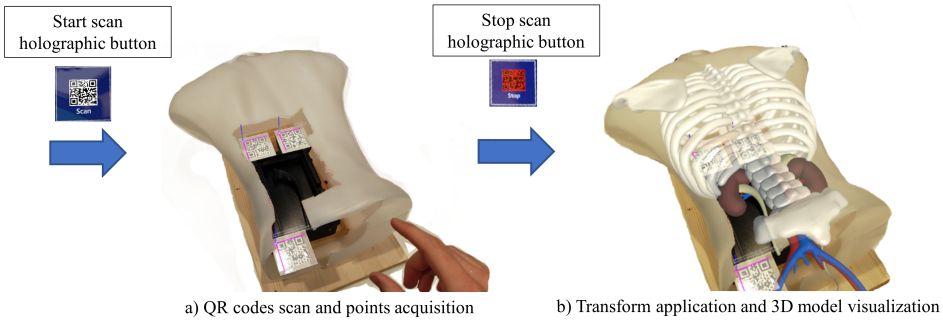

a) QR codes scan and points acquisition b) Transform application and 3D model visualization

Figure 2.11: Phantom registration workflow

2.2.1.1. Pre-planned Path Adjustment

As already mentioned in the System Framework, once the 3D model of the patient is visualized onto the real patient, the operator should be able to update the pre-planned insertion path by checking the intra-operative echographic images in order to not intersect fragile soft tissues that should not be touched from the insertion and that in the pre-operative images where not visible or not in the real location.
In order to implement this path update the augmented path visualized with the HoloLens has been set as interactable letting the operator move it by simply dragging a handle (see Figure 2.12).

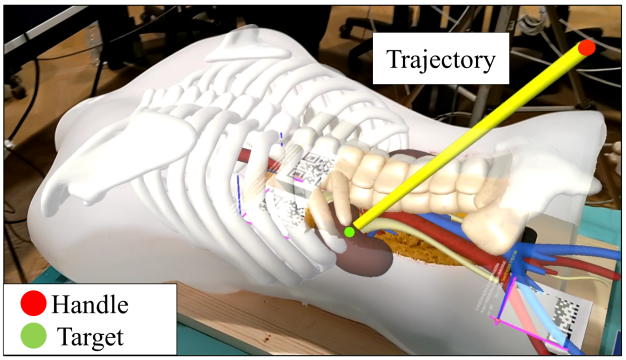

(a) Augmented trajectory visualization

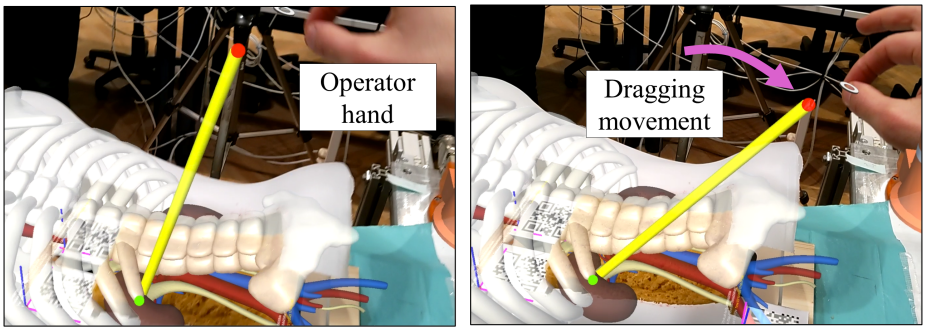

(b) Trajecotry update

Figure 2.12: Pre-planned path visualization and update

The strategy used to move the path, as implemented in the "PathRotation" Unity Script, is based on dragging the Handle (see Figure 2.12.b) and making the path follow it by rotating around the Target which becomes the pivot of the path rotation. In order to not let the user drag the handle out of reach with respect to the path, a built-in constraint furnished from the MRTK toolkit has been used, that fixes the distance of the handle from the Target to the radius R which in this case is $R = 300$ mm hence the length of the path.
Once the movement of the handle has been constrained to the space region where it can be

followed from the path, a strategy to make the path follow the handle has to be defined. In particular, the problem concerns the conversion of the cartesian coordinate of the handle into the angle of rotation of the path. This conversion has been achieved by implementing the cartesian to spherical coordinates conversion shown in Figure 2.13. By looking at the figure it can be seen that the cartesian position of the handle H corresponds to two angles of rotation (azimuth θ and inclination ϕ) of the vector $\vec{r}$. The solution is then to compute θ and ϕ starting from the Handle position H and apply these rotations to the path.

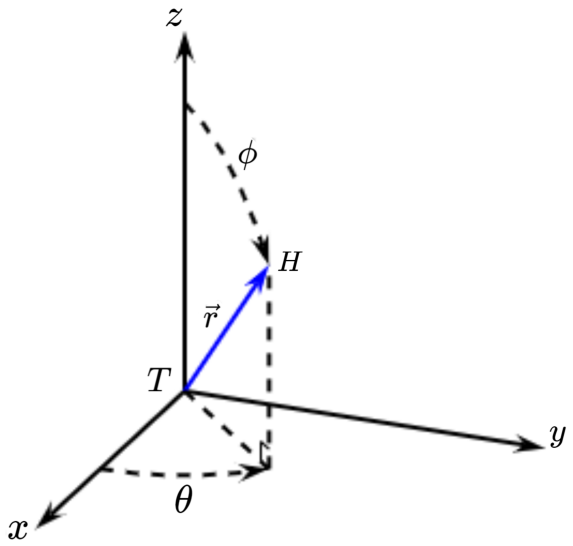

Figure 2.13: Cartesian and spherical coordinates representation

In order to obtain θ and ϕ starting from $H = (x, y, z)$ the following equations are applied:

$$\begin{aligned} \theta &= atan2(y, x) \\ \phi &= arccos(z/r) \end{aligned} \tag{2.5}$$

Then the rotations are applied to the path by applying θ rotation around z and ϕ rotation around the vector $\vec{v} = \vec{r} \times \vec{z}$, the final result will be the path following the handle H.

2.2.2. Robot registration

The robot registration, as mentioned in chapter 2.2, is the procedure to compute the coordinate transformation between the robot and the HoloLens (T^R_{Ho}). The procedure consists of computing the transformation T^R_{Ph}, since T^{Ph}_{Ho} is known from the phantom registration procedure stated above, the HoloLens to robot transformation can then be computed as $T^R_{Ho} = T^{Ph}_{Ho} \cdot T^R_{Ph}$.
The transformation T^R_{Ph} is computed by means of an Optical Tracker that is used to

compute both T_{OT}^{Ph} and T_{OT}^{R}, see Figure 2.14, that allows us to compute the desired transformation as $T_{Ph}^{R} = T_{OT}^{Ph-1} \cdot T_{OT}^{R}$

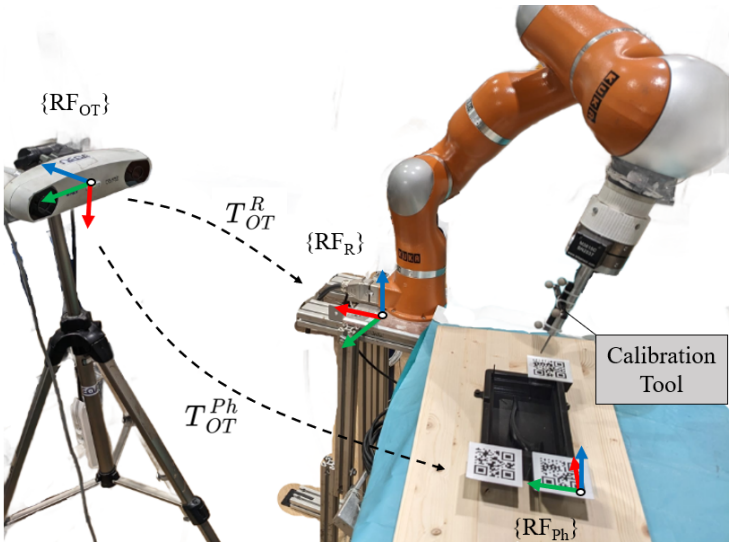

Figure 2.14: Robot calibration setup

As can be inferred from above, the robot registration procedure is divided into 2 steps: the OT to robot registration and the OT to phantom registration.

OT to Robot registration: implements the Eye-to-Hand calibration procedure [31], which is used to determine the transformation between a robot base and a sensor (in this case the Optical Tracker). In particular, the procedure allows the T_{OT}^{R} computation, blue transformation in Figure 2.15, by measuring T_{OT}^{Tool}, red transformation in Figure 2.15, by simply moving the robot in different configurations and using the forward kinematics to determine the robot base RF position and orientation.

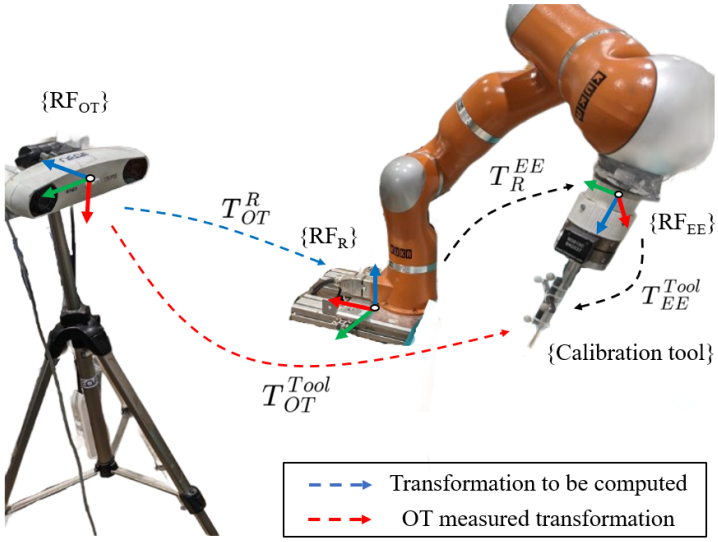

Figure 2.15: Hand Eye calibration RFs

In detail, the problem has the following mathematical formulation. For each robot configuration i, the T_{OT}^{R} transformation can be computed as

$$T_{OT}^{R} = T_{OT\ i}^{Tool} \cdot T_{Tool}^{EE} \cdot T_{EEi}^{R} \tag{2.6}$$

where T_{OT}^{Tool} and T_{EE}^{R} depend from the *i-th* robot configuration and T_{Tool}^{EE} and T_{OT}^{R} are constant. The Equation 2.6 can be treated in order to isolate the constant and unknown transformation T_{Tool}^{EE} in the following way:

$$T_{Tool}^{EE} = T_{OT\ i}^{Tool\ -1} \cdot T_{EEi}^{R\ -1} \cdot T_{OT}^{R} \tag{2.7}$$

The T_{Tool}^{EE} found in the Equation 2.7 is constant for each i, so the following system can be written:

$$\begin{cases} T_{Tool}^{EE} = T_{OT\ i}^{Tool\ -1} \cdot T_{EEi}^{R\ -1} \cdot T_{OT}^{R} \\ T_{Tool}^{EE} = T_{OT\ i+1}^{Tool\ -1} \cdot T_{EEi+1}^{R\ -1} \cdot T_{OT}^{R} \end{cases} \tag{2.8}$$

As a consequence of this equation system the unknown T_{Tool}^{EE} can be deleted by building the equation:

$$T_{OT\ i}^{Tool\ -1} \cdot T_{EEi}^{R\ -1} \cdot T_{OT}^{R} = T_{OT\ i+1}^{Tool\ -1} \cdot T_{EEi+1}^{R\ -1} \cdot T_{OT}^{R} \tag{2.9}$$

That then can be treated in order to have:

$$T_{EEi+1}^{R} \cdot T_{EEi}^{R\ -1} \cdot T_{OT}^{R} = T_{OT\ i+1}^{Tool\ -1} \cdot T_{OT\ i}^{Tool} \cdot T_{OT}^{R} \tag{2.10}$$

It can be noticed that the Equation 2.10 is in the form $AX = XB$, where $A = T^R_{EE\,i+1} \cdot T^{R\ -1}_{EE\,i}$, $B = T^{Tool\,-1}_{OT\ \ i+1} \cdot T^{Tool}_{OT\ \ i}$ and $X = T^R_{OT}$.
After moving the robot in N different configurations a set of N equations in the form of 2.10 is obtained. The mathematical equation $AX = XB$ is commonly the result of Hand-Eye calibration procedures so there are various methods available to solve it and achieve system resolution, in the current work, the Tsai algorithm is applied over the N equations, and the $X = T^R_{OT}$ is obtained.

These computations are performed in a Matlab script, that has as an input the transformation measured from the optical tracker (T^{Tool}_{OT}) and the KUKA robot joints values, needed to compute the T^R_{EE} transform with the robot forward kinematics. A detail to notice is that since a direct connection between ROS and Matlab has not been implemented, the joint values are retrieved from the ROS side passing by the HoloLens by using Robot-HoloLens connection of section 2.1.2 and then HoloLens-Matlab connection of section 2.1.3. These are the only two inputs needed from the Matlab script, each input has dimension N, which is the number of different robot configurations used, the higher N, the more accurate the Tsai algorithm result, so the better the estimation of T^R_{OT} is. In the specific application, $N = 80$ has been considered to be an appropriate number of configurations and they are all reached by moving by hand the robot set in gravity compensation control.

OT to Phantom registration: is used to compute the pose of the RF_{Ph} inside the RF_{OT} (hence the transform T^{Ph}_{OT}, see Figure 2.14). The procedure consists on the paired point registration between a set of points, which is a very similar approach to the one used in chapter 3.1.1. In this case, the difference is that 10 points, instead of 4, are used, so that the Singular Value Decomposition (SVD) method [32] returns a more accurate result. The 2 sets of 10 points used in the SVD method are with respect to RF_{OT} and RF_{Ph} and are the ones depicted in Figure 2.16.

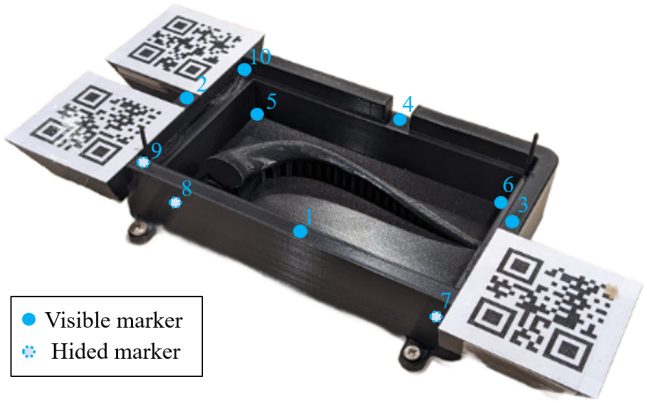

Figure 2.16: Position of the markers in the phantom

These points have known positions inside the phantom that define the set PhantomPoints = $\{M1_{Ph}, ..., M10_{Ph}\}$. The second set of the corresponding 10 points is given by the markers positions inside the RF_{OT} and is defined as OTPoints = $\{M1_{OT}, ..., M10_{OT}\}$. The OTPoints set is created by acquiring the 10 markers position with the Optical Tracker similarly as done in chapter 3.1.1.
The desired transformation matrix is then computed as:

$$T_{OT}^{Ph} = SVD(\text{PhantomPoints, OTPoints}) \tag{2.11}$$

2.2.2.1. Navigation system

The already mentioned systems of connection between HoloLens-Matlab-ROS (Section 2.1) and of robot registration (Section 2.2.2) allow the implementation of the real-time navigation system.
A navigation system that gives to the operator the perception of the position of the needle inside the patient would be a valuable feature for the system since it allows the operator to understand the distance from possible fragile structures, the correct performance of the insertion, and the perception of the moment when the needle touches the target.
The strategy to implement the navigation system is based on the visualization of the robot holographic twin superimposed onto the real one (Figure 2.17). This solution addresses the problem since during the insertion, even though the real robot tooltip won't be visible anymore, the holographic twin will give the perception to the operator of the correct position and orientation of the real needle.

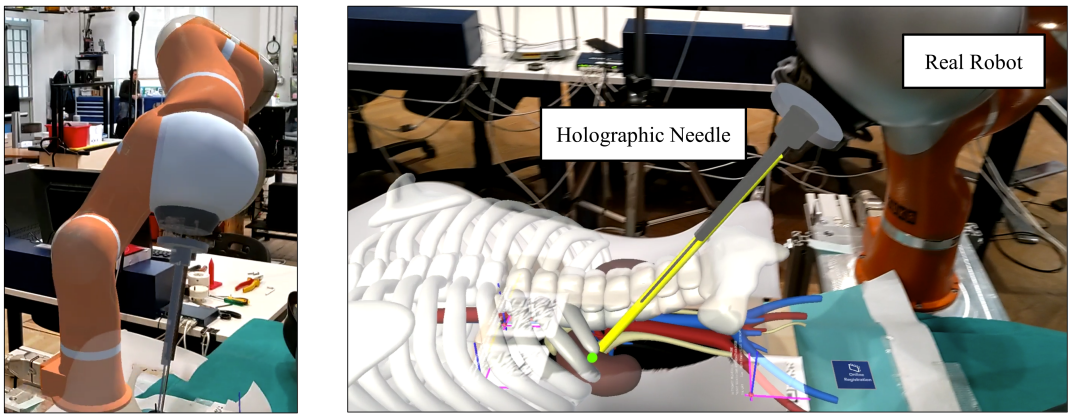

(a) Real and Holographic robot overlap (b) Navigation system during the PCNL

Figure 2.17: Holographic twin of the robot needle visualization

The navigation system is implemented thanks to two already implemented systems, as mentioned at the beginning of the section, in particular, the two systems are the (i) robot registration and the (ii) HoloLens-Matlab-ROS connection.

i. **Robot registration** permits to know the exact position of the robot base with respect to the phantom. Since the phantom position in the space is known thanks to the QR code scanning performed in the phantom registration procedure (2.2.1), the holographic twin of the KUKA robot can be visualized exactly in the position of the real one, resulting into the overlapping shown in the Figure 2.17.a.

ii. **HoloLens-Matlab-ROS connection** is fundamental in order to send the Robot registration result computed in Matlab (running on the Windows side), to the HoloLens and in order to emulate the real robot joints configuration retrieved from the ROS system onto the holographic twin .
Considering the robot registration result, once the data is sent, by following the procedure stated in the Matlab-HoloLens connection of Section 2.1, the position and orientation received from the HoloLens are applied onto the holographic twin of the robot inside the AR world.
Furthermore, the connection with the ROS system (as described in Section 2.1) is instead fundamental to update the holographic twin robot joint states, the final result of this connection is the perfect configuration emulation of the holographic robot as it can be seen in the Figure 2.17.a. The joints state update is continuously running during the procedure creating a real-time update of the holographic robot and allowing the navigation of the operator during the procedure (Figure 2.17.b).

2.2.3. Dynamic registration

One critical issue regarding the augmented reality visualization with the HoloLens is the hologram drift problem [33]. The drift is a phenomenon that causes an hologram to move away from where it was originally placed due to a lack of spatial anchors, long application running time, or big user movements inside the environment (for movement bigger than 5m from the initial position the HoloLens lose effectiveness). More in detail, the spatial anchors are objects in the field of view that, with their specific shape, work as a reference for the HoloLens environment scan and give to the glasses the possibility to compute their position in the space.
The drift problem could potentially limit the system's effectiveness due to the fact that surgeries could have long execution times, big surgeon movements, or not adapt spatial anchors.
The phantom registration as designed above, see registration workflow of chapter 2.2.1, is appropriate for the application startup and the initial QR code scanning. However, during the procedure, the surgeon is not able to stop the surgery workflow in order to do the QR codes scan whenever the drift of the hologram appears. In order to address this problem a dynamic registration strategy has been designed.
The dynamic registration strategy consists on continuous QR code scanning throughout the surgery and an easily reachable "Online Registration" button to update the position with the latest QR codes scanned.

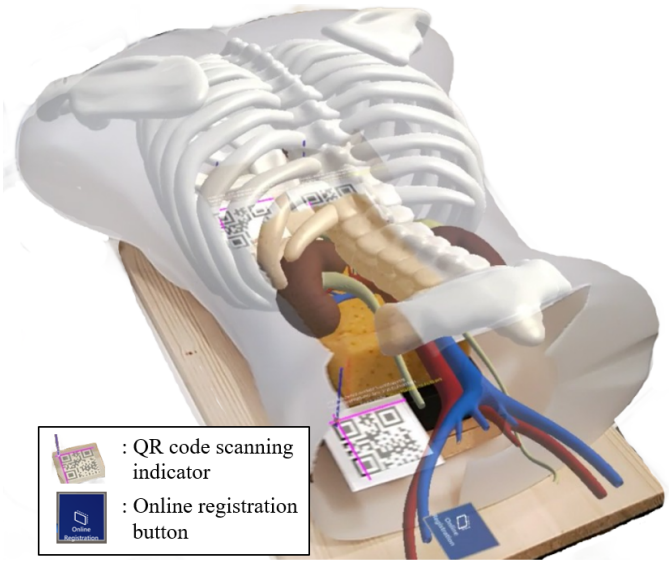

Figure 2.18: Dynamic registration graphic interface

As it can be seen in Figure 2.18, the "Online Registration" button is placed very close to

the surgeon's working field in a way to be easily pressed without making him distracted from the workflow. Alongside the button, also the QR code scanning feature can be seen, the purple indicator placed on the QR code signals to the surgeon the current position of the scanned QR code and that the online scanning is active. Whenever the surgeon feels the need to perform a new registration, he will simply need to make the QR codes enter in the HoloLens field of view, make them be scanned properly, and press the Online registration button. This procedure lasts around 10 seconds, doesn't make the surgeon move away from the working field, and doesn't cause the 3D model to disappear during the QR scanning.

2.3. Robot impedance control implementation

In this section, the robot control strategy implemented on the ROS side is presented. As mentioned above the control strategy implements the Cartesian Impedance Controller already present in the KUKA-lwr4+ robot.

Cartesian Impedance Control is a technique used to control robots as they interact with their environment. It models the robot's behavior as a spring and damper system, and determines how much the robot resists motion or force applied to it. Due to this property, this controller has been considered to be suitable for the current human-robot collaboration applications because properly setting the controller parameters would, limit the range of motion of the operator and force him to follow a predefined path.

The impedance control running in the KUKA lwr4+ can be expressed mathematically as a first-order differential equation that describes the motion of the robot's end effector (EE) in response to external forces. The equation takes the form:

$$k\delta x(t) + D\dot{x}(t) = F_{ext} \tag{2.12}$$

where $\delta x = (x(t) - x_0)$ is the displacement of the end effector position from a reference position x_0 at time t and $\dot{x}(t)$ is the velocity of the end effector. D and k are constants that describe the damping and stiffness of the robot at the current position $x(t)$, and F_{ext} is the external force applied to the end effector.

This equation shows that the motion of the robot depends on its stiffness and damping, depends also on the external force F_{ext} and that the robot force, the left side of the equation 2.12, depends on 2 different components: the spring force ($k\delta x(t)$) and the damping force ($D\dot{x}(t)$).

The system behavior can be explained by assuming that an external force, as the one the operator using the robot for the insertion procedure would impose, is applied onto the robot EE.
When a big enough external force F_{ext} is applied to the robot, the robot will start to move in response to the force. As the robot moves, the displacement $\delta x(t)$ in the formula will increase, causing the spring force $k\delta x(t)$ to increase. The increase in the spring force will cause the robot to resist further displacement and try to return to its original position x_0. The spring force linearly increments with the displacement so the bigger the move the harder the robot will be to move.
Moreover, the damping force $D\dot{x}(t)$ will increase as the robot's velocity $\dot{x}(t)$ increases. The damping force acts to resist the motion of the robot and slow it down, reducing the effect of the external force and the effect of the spring force oscillations.

As it can be inferred from the above explanation, an high stiffness value k would cause the robot to not move at all from the reference position x_0 even if a significant external force is applied. This is because the spring force $k\delta x(t)$ will be very large, and it will resist any attempt to displace the robot. This property has been used to avoid the operator from moving outside the predefined path by applying higher stiffness along the direction that would cause the robot to exit the path.

Controller parameters: The constants k and D are actually 6 dimensional vectors, $k = [k_x, k_y, k_z, k_{rx}, k_{ry}, k_{rz}]$ and $D = [D_x, D_y, D_z, D_{rx}, D_{ry}, D_{rz}]$, because formed from a component for each axis of the EE reference frame (RF_{EE} in Figure 2.19), in both linear and rotational movement. In this way, the 12 parameters cited above, regulate the behavior of the robot when an external force moves the robot EE from both an initial position and orientation. Moreover, the movement can be constrained differently depending on the direction along and around x,y and z of the RF_{EE}. This methodology has been utilized in the specific control strategy presented below.

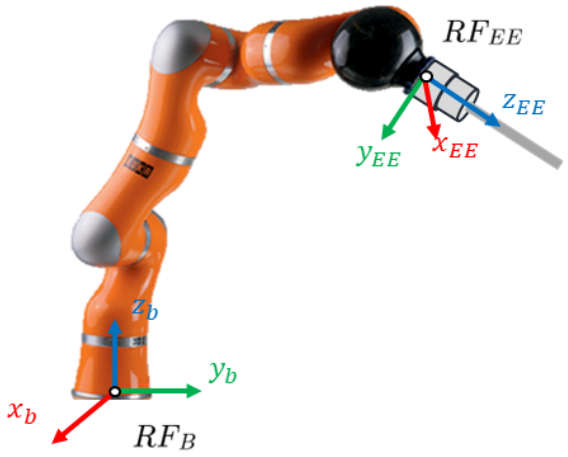

Figure 2.19: Base and EE reference frames positions and orientations

2.3.1. Proposed control strategy

As mentioned in the proposed framework, after visualizing the pre-planned path, the operator should be able to move the robot freely in order to align the ToolTip to the pre-planned path (Figure 2.20.a). Once the robot ToolTip is considered aligned, the operator has to press the "Robot Aligned" button in the AR graphic interface, consequently the robot movement will be constrained and the only movement allowed will be the one along the RF_{EE} z axis (Figure 2.20.b).

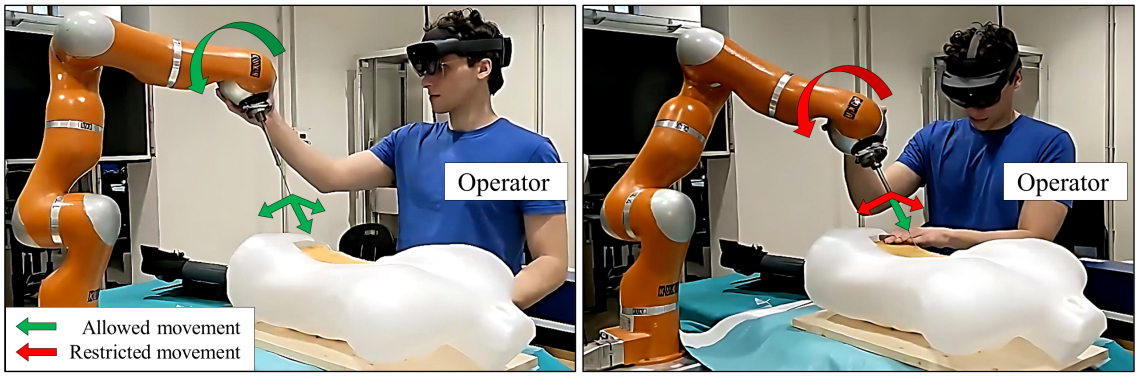

(a) Robot free movement (b) Robot constrained movement

Figure 2.20: The two robot movement modalities implemented in the system

Therefore, the two strategies implemented in the system by means of the application of the impedance control are the (i) free movement strategy and (ii) constrained movement strategy, both of them explained in detail below.

Free movement To obtain the free movement configuration the 12 parameters of k and D have to be assigned. All the stiffness parameters $(k_x, k_y, k_z, k_{rx}, k_{ry}, k_{rz})$ have to be small enough in order to keep the spring force $k\delta x(t)$ as small as possible and avoid the robot resistance to the movement along or around any axis but not too small in order to let the operator have smaller movement ranges and be able to accurately position the robot tooltip. In order to do so, the k range provided from the KUKA lwr4+ robot that goes from $k_{min} = 0$ to $k_{max} = 5000$ for k_x, k_y, k_z and from $k_{rmin} = 0$ to $k_{rmax} = 300$ for k_{rx}, k_{ry}, k_{rz} is considered.The k values are set to $k = [50, 50, 50, 10, 10, 10]$.

The damping parameters $(D_x, D_y, D_z, D_{rx}, D_{ry}, D_{rz})$ instead, are chosen in order to meet the "Critical damping" condition that sets the damping force just strong enough to stop the string-mass system from oscillating and just weak enough to avoid over-damping. In order to do so, the damping coefficient formula has to be considered:

$$D = 2\zeta\sqrt{k} \tag{2.13}$$

Where D is the damping coefficient that represents the level of damping force in the system, the higher the damping coefficient, the greater the damping force and the faster the oscillations will decay. Furthermore, the ζ is the damping ratio constant and k is the stiffness.
The "Critical damping" condition is reached if the damping ratio is equal to $\zeta = \frac{1}{\sqrt{2}} \simeq 0.707$. Consequently, the damping parameters D have been set in order to meet this condition considering that the parameters "2" and "$\sqrt{k}$" from the Equation 2.13 are automatically considered from the impedance control running in the KUKA lwr4+ robot making the final relation to be $D = \zeta$. Therefore, $D = 0.707$ has been assessed to be the final value to set.

The impedance controller script running in the ROS system when the robot is in free movement is simply setting the k and D parameters to the above-mentioned values. Alongside the parameters, the ROS script has also to update the x_0 position. By looking at the equation 2.3 in fact, it can be inferred that even if the stiffness is set to a small value, the robot will still be weakly attracted to the x_0 position initialized in the current position of the robot when the controller was started up. The consequences of this property of the impedance controller are two: (i) the robot is never completely free to move because for big displacement δx the spring force will be not negligible and (ii) the built-in impedance controller doesn't allow the robot to move with a $\delta x > 10$ cm in order to avoid big spring forces and consequent big robot speeds when the robot is released.

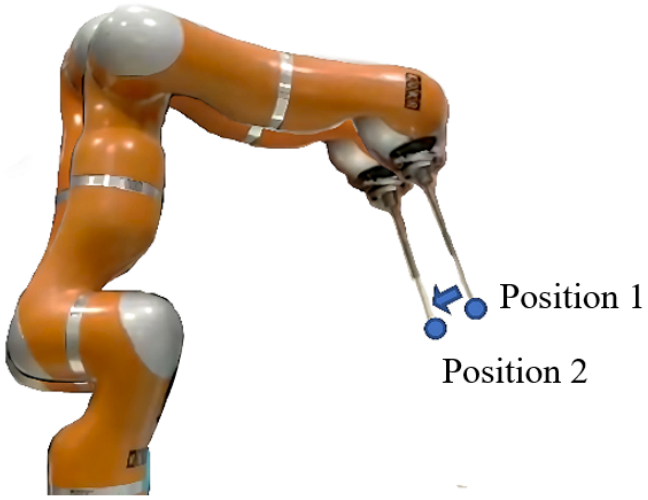

Figure 2.21: Schema of two different KUKA ToolTip positions

As a consequence of these two points, the result would be that the robot would be freely movable only inside a small range of 10 cm of radius around x_0.
The solution to this problem, as already mentioned, is to make the ROS script update the x_0 value every time the robot is moved (as shown in Figure 2.21, where X_0 passes by x_0 = Position1 to x_0 = Position2), in this way the displacement δx will always be smaller than 10 cm as far as the speed of movement won't be too big compared to the iteration rate of the script.
The ROS script running the impedance controller can be explained by looking at Figure 2.21. At the controller start-up the x_0 position is initialized at the first configuration tooltip position (x_0 = Position1), at the following script iteration, when the robot will be moved in the second configuration, the script will update the tooltip position to the new value (x_0 = Position2).

Constrained movement When the constrained movement is active the ROS script for the impedance controller sets different k and D parameters. The parameters are set in order to avoid the movement along x and y axis of the RF_{EE}, to avoid any rotation, and to let only the movement along z to occur. Following all the considerations done so far the following k and D values are set: $k = [4500, 4500, 1, 200, 200, 200]$ and $D = 0.707$. The k_x,k_y,$k_r x$,$k_r y$,$k_r z$ values can be interpreted as the maximum possible stiffness values with a big enough safe distance from the limit of the working field of the impedance controller (values too close to k_{max} would bring in some not ideal behavior from the spring behavior

of the robot), the k_z value is instead the smallest possible value of stiffness excluding the value of $k_z = 0$ that would bring as well some not ideal behavior from the robot. The damping parameter is set again equal to 0.707 for the same reason stated in the free movement strategy.

For the same reason stated in the free movement strategy, the x_0 position has to be updated for each movement of the robot (as shown in Figure 2.22, where x_0 has to pass by $x_0 =$ Position1 to $x_0 =$ Position2$_{updated}$ instead of Position2 as in the case of the free movement). However, since the movement is allowed to move only along the RF_{EE} z-axis the position update has to occur only along the RF_{EE} z-axis as shown in Figure 2.22.

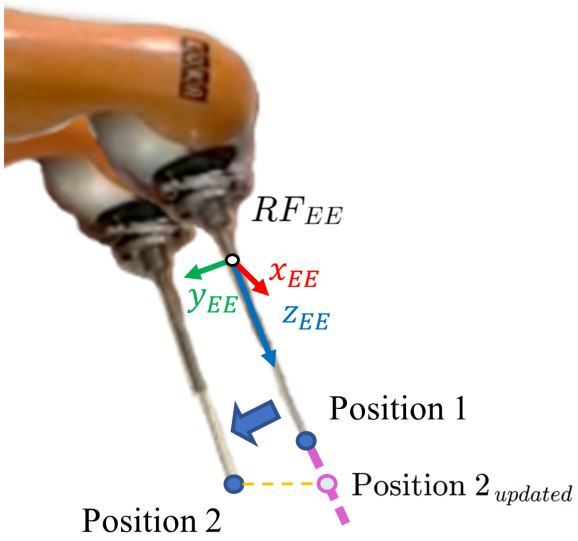

Figure 2.22: Schema of two different KUKA ToolTip positions and z-axis movement update

The coordinates of the points in the figure can be explained as:

$$\begin{aligned} &\text{Position } 1 = (x_1, y_1, z_1), \\ &\text{Position } 2 = (x_2, y_2, z_2), \\ &\text{Position } 2_{updated} = (x_1, y_1, z_2) \end{aligned} \tag{2.14}$$

Where all the points coordinates are expressed with respect to the RF_{EE} shown in figure 2.22. From this equation system it can be seen that the only parameter to be updated after the movement of the robot is the z.
The behavior corresponding to the k and D parameters set above alongside the z-axis

update as just mentioned corresponds to a free and limitless movement of the robot EE only along the RF_{EE} z-axis while any movement along x and y would encounter a high stiffness that would prevent big movements and the absence of x and y update would attract the robot back to x_1 and y_1 after the external force stops.

z-axis update coordinate transformation Even though the built-in impedance controller is set onto the RF_{EE} and the k and D parameters work along and around the x, y and z axis of the EE, the x_0 position update along the RF_{EE} z-axis is not equally straight forward. The end-effector position, as retrieved from the /pose/end_effector topic in the ROS system, is with respect to the reference frame of the robot base (RF_B in Figure 2.19), not with respect to RF_{EE}. For this reason, a coordinate transformation is needed to map the x_0 position from the RF_B to the RF_{EE}, apply the z-axis update, and map it back to the RF_B. The mathematical procedure followed in the ROS script is described below.

Let's consider the robot tool tip starting position as P_1 (Position 1 in Figure 2.14), when an external force is applied to the robot a displacement of the tooltip position occurs, let's call this second position P_2 (Position 2 in Figure 2.14). The two point coordinates can be expressed both in the base reference frame (P_1^B, P_2^B) and in the end-effector reference frame (P_1^{EE}, P_2^{EE}).
The procedure is performed as follows:
the two points are mapped into the RF_{EE} by means of the equations:

$$\begin{aligned} P_1^{EE} &= R_{EE}^B \cdot P_1^B - R_{EE}^B \cdot T_B^{EE} \\ P_2^{EE} &= R_{EE}^B \cdot P_2^B - R_{EE}^B \cdot T_B^{EE} \end{aligned} \tag{2.15}$$

Where R_{EE}^B and T_B^{EE} are known from the ROS topic "/pose/end_effector" that gives the rotation and position of the EE in the robot base reference frame. Once the two points have been computed, the vector between these two is built:

$$\overline{v} = \overline{P_1 P_2}^{EE} = (v_x, v_y, v_z) \tag{2.16}$$

Then the x and y components are removed in order to create the point $P_{2updated}^{EE}$ that updates only along z:

$$P_{2updated}^{EE} = P_1^{EE} + (0, 0, v_z) \tag{2.17}$$

It can be noticed that since the vector $\overline{v}$ is mapped into the RF_{EE} the new point $P_{2updated}^{EE}$ corresponds to the P_1 translation along the RF_{EE} z-axis.

The final step is to map the updated position $P^{EE}_{2updated}$ back to the base reference frame as:

$$P^{B}_{2updated} = R^{EE}_{B} \cdot P^{EE}_{2updated} + T^{EE}_{B} \tag{2.18}$$

$P^{B}_{2updated}$ is the $P_{2updated}$ position in the base reference frame as requested from the impedance controller script.

2.4. Experiment protocol

The above sections are enough to implement a functioning system, this last section has been designed to test the validity of the system, to see if it brings advantages with respect to the currently used method in the operating rooms and how it performs with respect to other similar system considered in many grey literature studies in the field of AR assisted needle insertion procedures.

2.4.1. Experiment setup

This section provides an explanation of the system's validation modalities, outlining the user testing procedures conducted on the system.
User testing is a crucial aspect of this study because the implementation of an AR visualization system is expected to have a subjective impact on the procedure's execution. As previously noted, this final section aims to evaluate the system's performance and compare it to the current method used in the operating room, as well as other grey literature studies that have investigated AR-assisted insertion procedures. Based on these studies, the most commonly used performance metrics to evaluate these types of systems are both objective measurements of insertion accuracy with respect to a reference path, as well as subjective user experience evaluations conducted through the use of user questionnaires.

User study In order to evaluate the metrics stated above the following user study modality has been defined.
To ensure statistically reliable results, a group of 14 participants was selected for user testing. All participants had no prior surgery training and were not familiar with the system, the HoloLens, or the robot. Each of them was asked to perform the same insertion procedure on the specified phantom model using four different system setups in random order. The insertion procedure was repeated three times for each setup. The four setups were designed to provide a clear understanding of the distinct impact of the two main contributions of the current work: AR visualization and Robotic Assistance.
The 4 setups are the following ones:

- **Screen:** 2D screen visualization and manual insertion
- **Screen + Assistance:** 2D screen visualization and robotic-assisted insertion
- **AR:** 3D Augmented reality visualization and manual insertion
- **AR + Assistance:** 3D Augmented reality visualization and robotic-assisted insertion

The expectations are to obtain a better performance with the AR visualization compared to the 2D screen one and to have a better performance with the Robotic assistance insertion with respect to the manual one. To provide further detail, the expected performance outcomes for the above-mentioned setups are as follows:

- The combination of screen and assistance would have better results than using only the screen.
- The use of AR in combination with assistance would have better results than using AR alone.
- The use of AR alone would have better results than using only the screen.
- The combination of AR and assistance would have better results than using the combination of screen and assistance.
- The combination of AR and assistance would have better results than any of the other systems.

User study framework For the sake of simplicity in explaining the user study framework, the AR + Assistance setup will be used as the reference point. From this setup, all subsequent modifications to the system to obtain the other setups will be explained.
The AR + Assistance setup is very similar to the System framework explained in the Introduction with some modifications explained below.

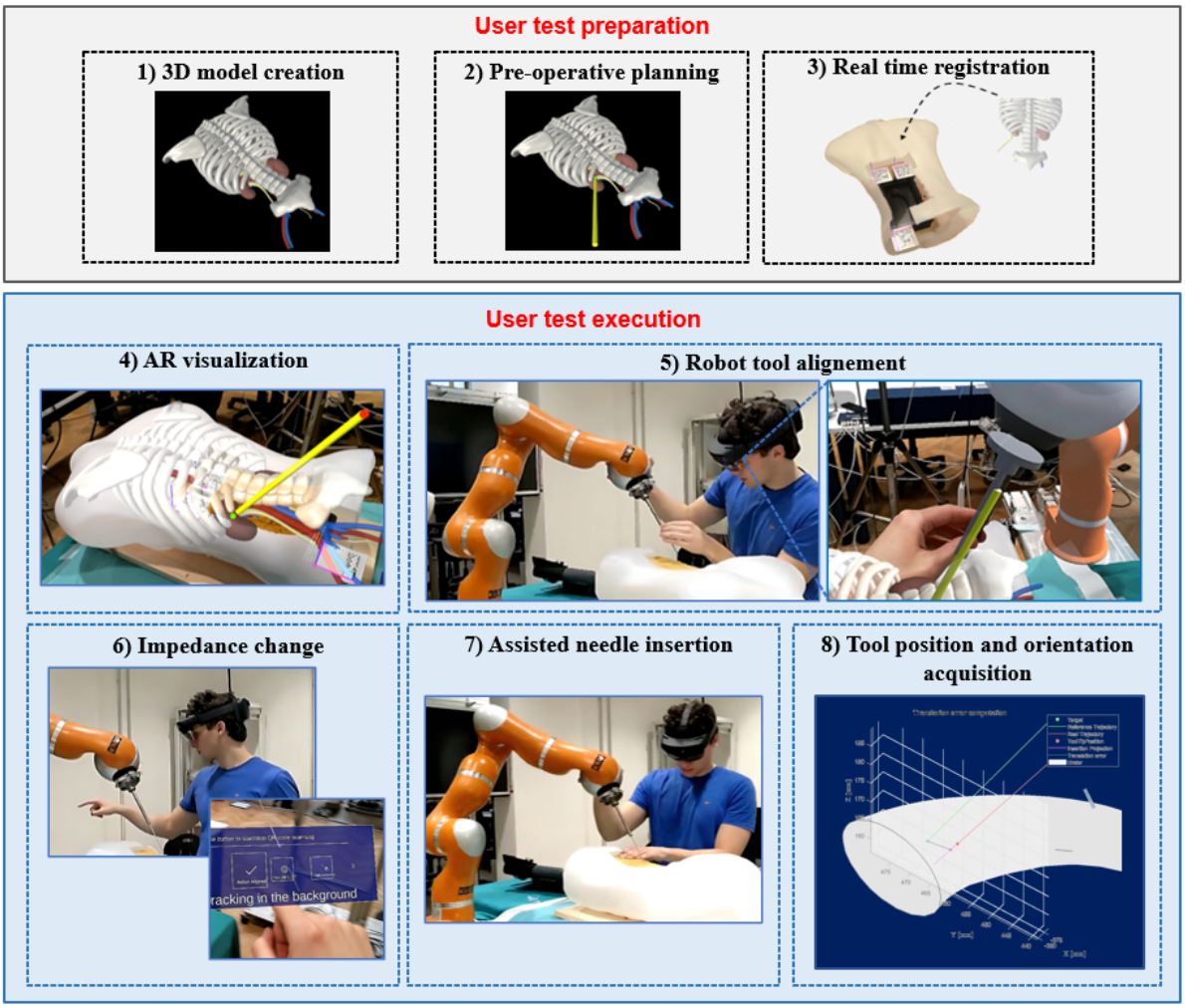

Figure 2.23: AR + Assistance user test framework steps

The steps of the AR + Assistance user test framework depicted in Figure 2.23 are the following:

- **Preparation:** It is the phase in which the setup for the user test is prepared, more precisely it accounts for the pre-operative planning that sets the reference path on which the insertion accuracy will be evaluated, and the real-time registration.
- **Execution:** This phase involves the user performing the insertion process. Once the augmented path is displayed (Step 4), the user manually aligns the holographic robot tooltip to the augmenter path (Step 5). When the alignment is deemed satisfactory, the user presses the "robot aligned" button in the AR graphic interface (Step 6), causing the robot to change stiffness as described in previous sections. Then, the user simply needs to push the robot along the fixed direction to perform the insertion (Step 7). When the user indicates that the tool has made contact with

the ureter, the tool's position and orientation are saved (Step 8).

As already mentioned this is the framework that explains the AR + Assistance setup, the other three cases can be explained as follows:

- AR: All steps remain the same, except for the exclusion of Step 6. This means that the robot does not assist the insertion in Step 7 and the operator has to be as focused as possible on not changing the ongoing insertion path once entered in the manikin, this is done to simulate the real surgery scenario. The result is a fully manual maneuver.
- Screen + Assistance: All the steps remain the same but the modality of visualization of the model changes from implementing the AR to using a 2D screen.
- Screen: All steps remain the same, except for the change in the visualization modality and the exclusion of Step 6. This means that the robot does not assist the insertion in Step 7 and the same attention over the ongoing insertion path of the case "AR" has to be taken. The result is a fully manual maneuver.

It is important to specify that the screen visualization was achieved by running the HoloLens application in the Unity editor. Essentially, the same software that was used to program the application can simulate the app and display all the elements of the augmented reality environment on a computer screen.

Operating room simulation As previously stated, the objective of the experimental validation is to compare the benefits of AR visualization and robotic assistance with the current PCNL setup used in the operating room. To facilitate this comparison, the operating room setup was closely replicated. This involved emulating the visualization modalities utilized in the operating room.

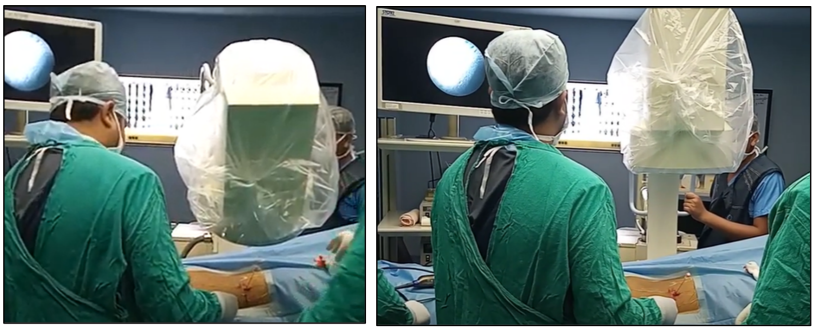

(a) Operating room visualization

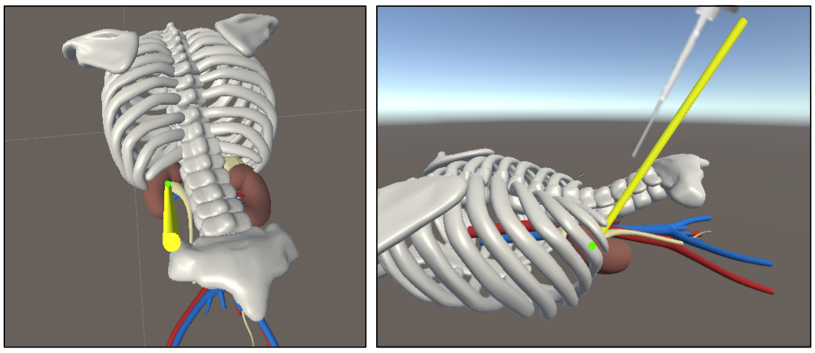

(b) Emulated screen visualization

Figure 2.24: Screen visualization modality

Figure 2.24.a illustrates the two distinct perspectives of the target that are assessed via fluoroscopic imaging during the PCNL procedure. These perspectives include both a top and side view. The screen view simulation depicted in Figure 2.24.b is an application of these above-mentioned top and side views.

2.4.2. Performance metrics

The evaluation of performance metrics is a crucial aspect of assessing the effectiveness of medical interventions and surgical techniques. This section outlines the specific performance metrics employed in the study. Through an examination of these metrics, we can make conclusions regarding the benefits and drawbacks of each setup and determine whether AR visualization and robotic assistance present improvements over the current PCNL approach.

As previously noted, the potential subjective impact of AR visualization on individual users necessitates a user experience evaluation in addition to a more objective accuracy evaluation. Therefore, the two performance metrics used in the evaluation are the following ones:

- User questionnaire
- Insertion error
- Time

User questionnaire Is the evaluation performed in order to understand the usability of the system which is an indication of the effort required. The test conducted for this statistical analysis was the NASA Task Load Index (NASA-TLX). This index rates the perceived workload when assessing a task and it is calculated on the basis of a questionnaire that is filled in by the users after having performed the task with every system setup. The questionnaire is based on six questions about Mental Demand, Physical Demand, Temporal Demand, Performance, Effort, and Frustration, each rated from 1 to 20. After users complete the NASA-TLX questionnaire, their responses for each of the six categories, are analyzed using box plots and their relative p-values. Additionally, an overall score is calculated by summing up the scores from each category that has been analyzed as well.

Box plots provided a more qualitative and intuitive way to compare the different system setups, by directly comparing the median errors and their distributions. This approach allowed us to identify any significant differences in performance between the system setups, and to gain a better understanding of how the different factors affected the accuracy of the system.

Even though boxplots provides a visual summary of the distribution of the data, and can help to identify differences between groups or samples, it does not provide a formal statistical test of significance. To determine whether the observed differences between groups or samples are statistically significant, a hypothesis test is conducted using the p-value computation. The p-value significance level has been set to 3 different values, in the way to determine the grade of statistical significance of every comparison. The 3 levels are $p<0.05$, $p<0.01$, and $p<0.001$ (respectively indicated with *,**, and *** in the p-values tables indicated below).

On the other hand, the mean and standard deviation analysis was used to understand the results from an absolute point of view and to compare the system results to other studies in the literature that focused on the topic of needle insertion. This approach allowed us to quantitatively assess the differences between the system setups and to provide a baseline for comparison with other studies.

Insertion error The insertion error has been evaluated by using the common metrics used in the grey literature for needle insertion tasks. In particular, the two values taken into account are the translation error with respect to the target position and the orientation error with respect to the reference path orientation.
More in detail, the translation error could not be computed as most studies in the field do, by simply computing the Euclidian distance between the final tooltip position and the target (see figure 2.25), the reason is that the target is inside the 3D printed ureter and it could not be perforated. To solve this problem the strategy implemented in different studies such as [28] of projecting the tooltip position along the insertion path has been implemented (see Figure 2.25), the translation error can be computed as the distance between the target and the projection. With this strategy both the orientation error (E_O) and the translation error (E_T) can be computed as follows:

$$\begin{aligned} E_O &= acos(\frac{\vec{v}_{planned} \cdot \vec{v}_{real}}{\|\vec{v}_{planned}\| \cdot \|\vec{v}_{real}\|}) \\ P &= |\vec{v}_{planned}| \cdot cos(\alpha) \cdot \vec{v}_{real} \\ E_T &= \|P - T\| \end{aligned} \tag{2.19}$$

Where, $\vec{v}_{planned}$ is the vector representing the direction and the magnitude of the reference path, $\vec{v}_{real}$ represents the real insertion procedure path performed by the user, α is the angle between the two vectors and P is the closest point to the target belonging to the insertion path.

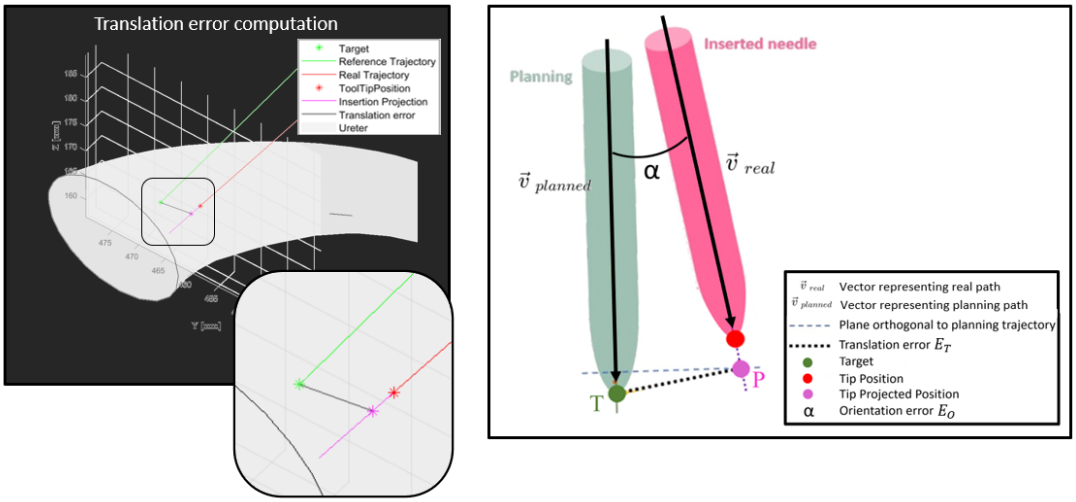

(a) Insertion error Matlab output

(b) Insertion error detailed schema

Figure 2.25: Translation error evaluation

It is important to notice that this modality of translation error measurement is compatible

with the surgery requirements. PCNL insertion procedure is performed to create a pathway to the ureter, rather than directly to the stone itself. Once the pathway is created, a nephroscope equipped with a camera is used to access the stone within the ureter. During this stage of the procedure, the surgeon also adjusts the depth of the positioning, which means that the previous needle insertion procedure's positioning has to be accurate for lateral placing only.
These two values are computed starting from the acquisition of the tooltip position and orientation from the $\backslash pose \backslash tool\_tip$ ROS topic from the ROS system. The pose and orientation obtained are inputted in the Matlab script that thanks to the robot registration performed in the section 2.2.2 can compute the position of the tooltip with respect to the ureter (see the output of the Matlab script in Figure 2.25.a). The computations as specified in the equations 2.19 are then performed and the resulting errors E_T and E_O are saved.
At the end of all the user tests 3 E_T and 3 E_O for each user in each system setup have been gathered creating the dataset on which to perform the statistical analysis. The statistical analysis consists of the mean value and standard deviation computation over all the user errors differentiated for each system setup and a box-plot analysis with the relative p-values computation for the systems performance comparison.

Time cost In order to have a more objective indication of the time demand of the system, the time to perform the operation has been acquired. The time spent on a surgical procedure has a big impact on patient safety, resource utilization, surgeon performance, and patient comfort. Therefore, measuring and analyzing the time of execution of surgery can provide important insights into the quality of care provided. The strategy to acquire it consisted of measuring it with the stopwatch between the initial instant of the procedure (with the robot in a standard not aligned initial position) and the final one (corresponding to when the tool tip touches the ureter). All the times of execution are then averaged for all the users over the same system setup and the boxplots with the relative p-values are compared.

3 | Results

In this section, the performance metrics results of the work are presented alongside their interpretation, the aim is to investigate the advantages and limitations of two main contributions - augmented reality visualization and robotic assistance - compared to the standard percutaneous nephrolithotomy procedure.
The results are presented in two main parts. The first part presents the registration methods' accuracy that directly affects the overall system. The second part presents the overall system performance analysis evaluated with the method already explained in the section 2.4.1.
At the end of the section, there will be the interpretation of the results concluding with the analysis of the benefits and drawbacks of the system and the comprehension of the work contribution to the PCNL procedure field.

3.1. Registration accuracy results

The minimum accuracy needed for a PCNL needle insertion procedure will depend on several factors, including the size and location of the stone, the skill level and experience of the surgeon performing the procedure, as well as the registration accuracy if the current system is employed. Generally speaking, a needle insertion accuracy of within 2-3 mm from the stone is considered acceptable for PCNL procedures.

3.1.1. Phantom registration

The phantom registration accuracy has been verified in order to understand the error in the placement of the holographic model onto the real patient. The evaluation method design, inspired by the study [34], and its results are discussed below.

Evaluation method design: in order to evaluate the error in the estimation of the T_{Ho}^{Ph} transformation, 4 markers whit known positions have been defined in the phantom RF. 4 holographic spheres have been placed in the RF_{Ho} at the same position of the markers and the T_{Ho}^{Ph} has been applied to them. The error in the overlapping of the real

and holographic markers depends on the registration accuracy.

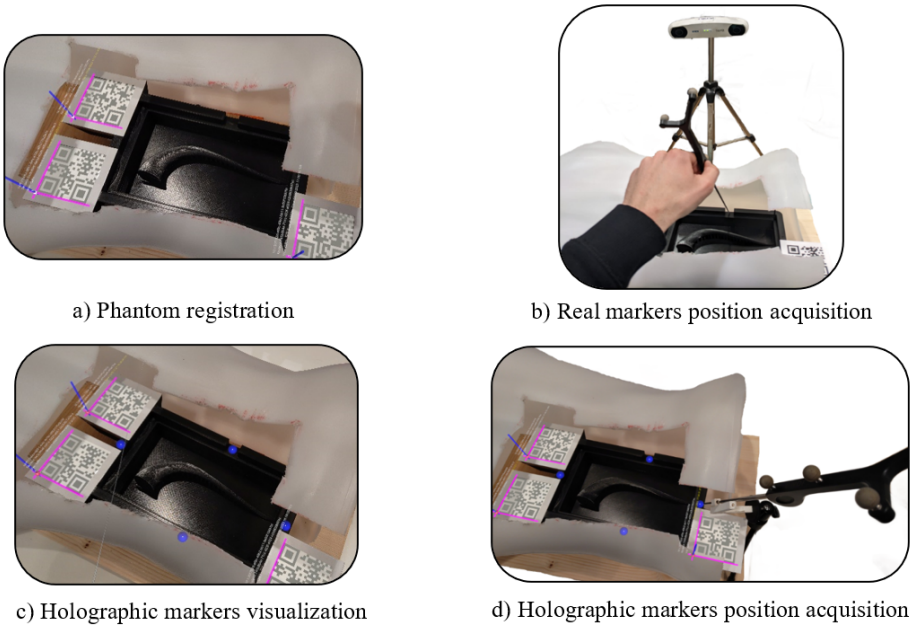

Figure 3.1: Markers error evaluation

The markers overlapping error is then measured by implementing an Optical Tracking device that acquires the position of each marker 50 times, see Figure 3.1.b and 3.1.d. After the acquisition an average is applied to the 50 acquisitions and the result is saved. The average is computed in order to delete noises in the measurement. The markers' positions are then sent to a Matlab script that saves them as realMarkers = $\{M1_{Real}, M2_{Real}, M3_{Real}, M4_{Real}\}$ and holoMarkers = $\{M1_{Holo}, M2_{Holo}, M3_{Holo}, M4_{Holo}\}$, and performs the computations.

The computations performed on these two sets of points are of two types: i) Euclidean distance computation for each marker and ii) root mean squared error over some ureter vertices positioning errors. The second method has been defined because the registration error is not uniform over the whole space and the most relevant overlapping error is at the level of the ureter, since it is the focus of the surgical procedure, achieving an acceptable level of error in this area ensures the overall success of the registration procedure.

i **Markers Euclidean distance computation:** is the simple Euclidean distance computation for each marker, following the formula:

$$E_i = \|Mi_{Real} - Mi_{Holo}\|, i = 1, ..., 4 \tag{3.1}$$

The resulting errors are: $E_1 = 3.1856$ mm, $E_2 = 1.7835$ mm, $E_3 = 3.6304$ mm and $E_4 = 3.5982$ mm.

ii **Ureter vertices root mean squared error:** In order to compute this value some ureter vertices' positions had to be defined in the Matlab script. Their positions have been extrapolated from the phantom 3D model, in which the ureter mesh position is known with respect to the RF_{Ph}. These data are then saved in Matlab as CTvertices. The CTvertices positions are saved in the script with respect to the Optical Tracker RF (RF_{OT}) so a transformation is needed to know the position of both the phantom vertices (T_{OT}^{Ph}) and holographic vertices (T_{OT}^{Ho}).

T_{OT}^{Ph} and T_{OT}^{Ho} computation: to compute these two transformations the Singular Value Decomposition (SVD) algorithm is applied over the markers. In fact, the markers position are known with respect to the RF_{OT}. Consequently, the SVD algorithm can be performed over the 2 couples of paired points to compute the two transformations:

$$\begin{aligned} T_{OT}^{Ph} &= SVD(\text{CTmarkers, realMarkers}) \\ T_{OT}^{Ho} &= SVD(\text{CTmarkers, holoMarkers}) \end{aligned} \tag{3.2}$$

Once these two transformations are computed, the CTvertices are transformed in both holoVertices = $T_{OT}^{Ho}*$ CTVertices and realVertices = $T_{OT}^{Ph}*$ CTVertices. The RMSE is then computed over the two sets of vertices, which can be visualized in the Figure 3.2.a, with the formula:

$$RMSE = \sqrt{\frac{1}{N}(\text{realVertices - holoVertices})^2} \tag{3.3}$$

Where N is the number of points inside the sets: realVertices and holoVertices and in the Matlab code is set to 20.

Results: the RMSE results to be (boxplot in the figure 3.2), hence an acceptable value if compared to the state of the art that for example in the study [35] is of 2.7mm and in the study [34] is of 3.19mm. Moreover, the RMSE is significantly lower than the error of the markers' positioning, which resulted to be around 3mm on average, this can be explained by the position of the QR Codes used to make the registration. These QR Codes are in fact placed in order to surround the target of the surgery, hence the ureter, and it is proven that a higher registration accuracy is reached at the center of the distribution of the points used for the registration, hence the accuracy is higher in the target location.

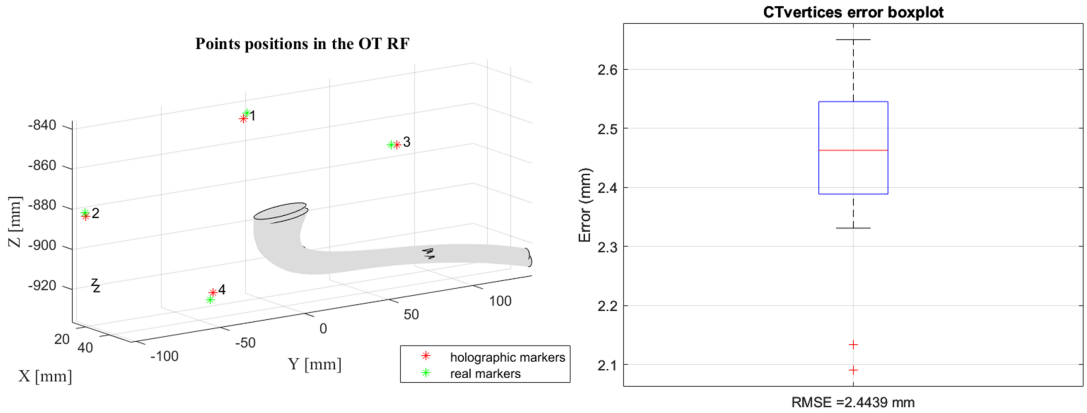

Figure 3.2: Real and holographic ureter overlapping error

3.1.2. Robot registration

Once the robot to phantom transformation has been computed with the chain rule of the two above-computed transformations ($T^R_{Ph} = T^{Ph-1}_{OT} \cdot T^R_{OT}$) the accuracy of the registration result has to be evaluated.

Evaluation method design : In order to evaluate the T^R_{Ph} transformation accuracy the following method, taken from gray literature [28], as been implemented.
The more the T^R_{Ph} transformation is accurate, the more the transformation applied to the markers' positions with respect to the phantom RF is similar to the same marker position inside the robot RF (RF_R). Therefore, let's define Mi_R as the *i-th* marker position in the RF_R measured by reading the ToolTip pose topic from ROS when the robot is positioned as in Figure 3.3. Let's define Mi_{Ph} as the known position of the same marker in the RF_{Ph}, then the *i-th* marker positioning error can be computed as:

$$E_i = |Mi_R - T^R_{Ph} \cdot Mi_{Ph}| \tag{3.4}$$

The E_i is computed over the markers number 1,2,3 and 4 (see Figure 2.16) and then the RMSE is computed over these 4 errors as:

$$RMSE = \sqrt{\frac{E_1^2 + E_2^2 + E_3^2 + E_4^2}{4}} \tag{3.5}$$

Figure 3.3: Marker position acquisition with the robot

The resulting RMSE is equal to 1.4862mm (Figure 3.4). The result is also comparable with the current state of the art and even better than some solutions that don't implement the Optical Tracker, which is a very precise measurement tool, like in the case of paper [4] or [28] where the accuracy has an average value of 3.36 mm.

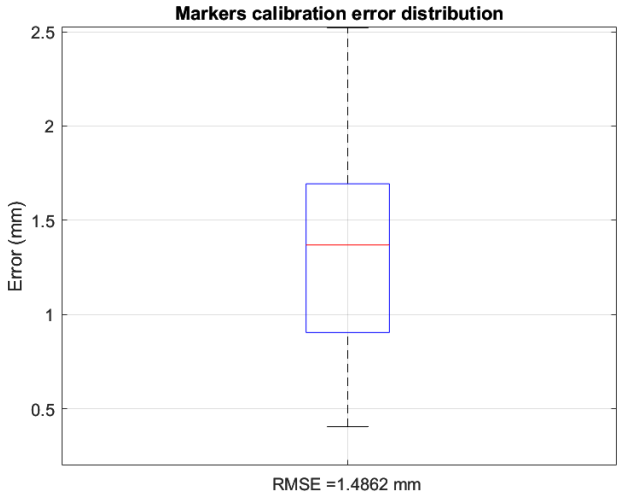

Figure 3.4: Phantom to robot registration error boxplot

3.1.2.1. Holographic robot alignement

An important observation to make is the fact that the two registration errors computed above combine together when performing the needle insertion by aligning the real robot

to the holographic path. This happens because the positioning between the holographic model and the real robot is the given by $T^R_{HO} = T^{Ph}_{Ho} * T^R_{Ph}$ so there is the error propagation phenomenon.
In order to avoid this problem the holographic twin of the robot already implemented in the system has been used. In fact, if for the alignment procedure, the holographic twin of the robot is used instead of the real one, the error given by the phantom registration can be neglected resulting in a more accurate insertion.

3.2. Comparison experiment results

This section presents the results of the analysis conducted on the system using the methodology described in Section 2.4.1. The evaluation metrics that were assessed include both objective performance measures (accuracy of performance and time of execution) and subjective measures (user experience and system usability). The results for each of these sections are presented separately below.

***E_T* and *E_O* errors and execution time** As previously mentioned in Section 2.4.1, each of the 14 users was asked to perform the same PCNL insertion procedure three times for each system setup, resulting in a dataset of 12 E_T, 12 E_O and 12 $Times$ measurements per user. To ensure statistical validity and meaningful conclusions, the results for each user were combined and separated according to the respective system setups. The final dataset then was organized to include 42 E_T, 42 E_O, and 42 $Times$ measurements per system setup, regardless of the specific user that performed the insertion.
By aggregating the results in this way, we can analyze the performance of the different system setups in a more robust and comprehensive way while minimizing the subjective variations introduced by each user.

Once the 3 datasets of 42 elements for each system setup were obtained, we conducted two types of evaluation: box-plot analysis, and mean and standard deviation computation. These two approaches had different objectives and provided complementary insights into the performance of the system setups.

The two evaluation methods output as computed from Matlab are the following ones:

i. Box-plot:
   The box plot of the 4 different system setups are the following ones:

p - values				
Metrics	**Setups**	*Screen + Assisted*	*AR*	*AR + Assisted*
O error	*Screen*	9.6507e-07 (***)	0.5512	1.8359e-11 (***)
	Screen + Assisted	-	3.1381e-04 (***)	0.0471 (*)
	AR	-	-	1.4834e-08 (***)
T error	*Screen*	0.0165 (*)	0.9575	2.5524e-13 (***)
	Screen + Assisted	-	0.0647	1.3699e-07 (***)
	AR	-	-	1.5915e-10 (***)
Time execution	*Screen*	0.0011 (**)	2.721e-10 (***)	0.0011 (**)
	Screen + Assisted	-	1.254e-04 (***)	0.8022
	AR	-	-	4.2968e-04 (***)

Table 3.1: Translation and Orientation error, and execution time p-values

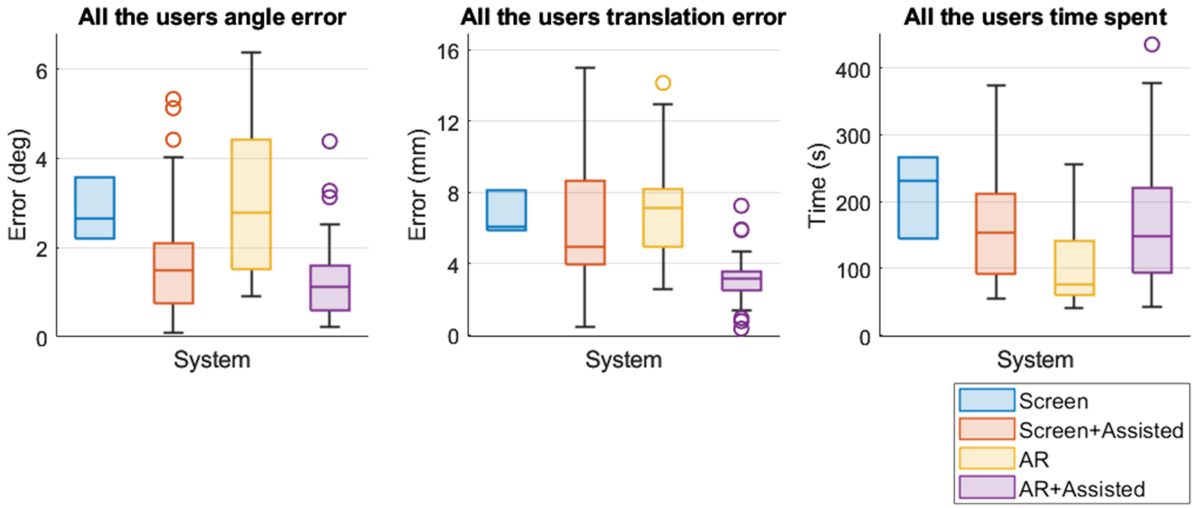

Figure 3.5: Translation and Orientation error, and execution time box-plots

ii. Mean and standard deviation:
The insertion errors and time of execution mean and standard deviation values are shown in the table below.
It can be noticed that each system setup's best value of every row is enlightened with bold text.

NASA Task Load Index As already mentioned, the usability of the system has been assessed with the NASA-TLX. All the user answers have been put together and then grouped depending on the system setup used. Alongside the specific NASA-TLX answers a

	Procedure setup							
	Screen		*Screen + Assisted*		*AR*		*AR + Assisted*	
Metrics	*Mean*	*SD*	*Mean*	*SD*	*Mean*	*SD*	*Mean*	*SD*
Exacution time [s]	*218*	*50*	*165*	*82*	***100***	***55***	*171*	*109*
Translation error [mm]	6.60	1.00	6.19	3.15	7.42	3.57	**3.17**	**1.36**
Orientation error [deg]	2.81	0.59	1.79	1.36	3.17	1.80	**1.24**	**0.88**

Table 3.2: T error, O error, and execution time mean and standard deviation values

new additional category has been added, the "overall" category that sums up all the other categories' scores and scales the result between 0 and 100. The NASA-TLx results have been evaluated only through the boxplot due to the qualitative nature of the questionnaire more quantitative assessments were not considered valuable.
The resulting boxplot are the following:

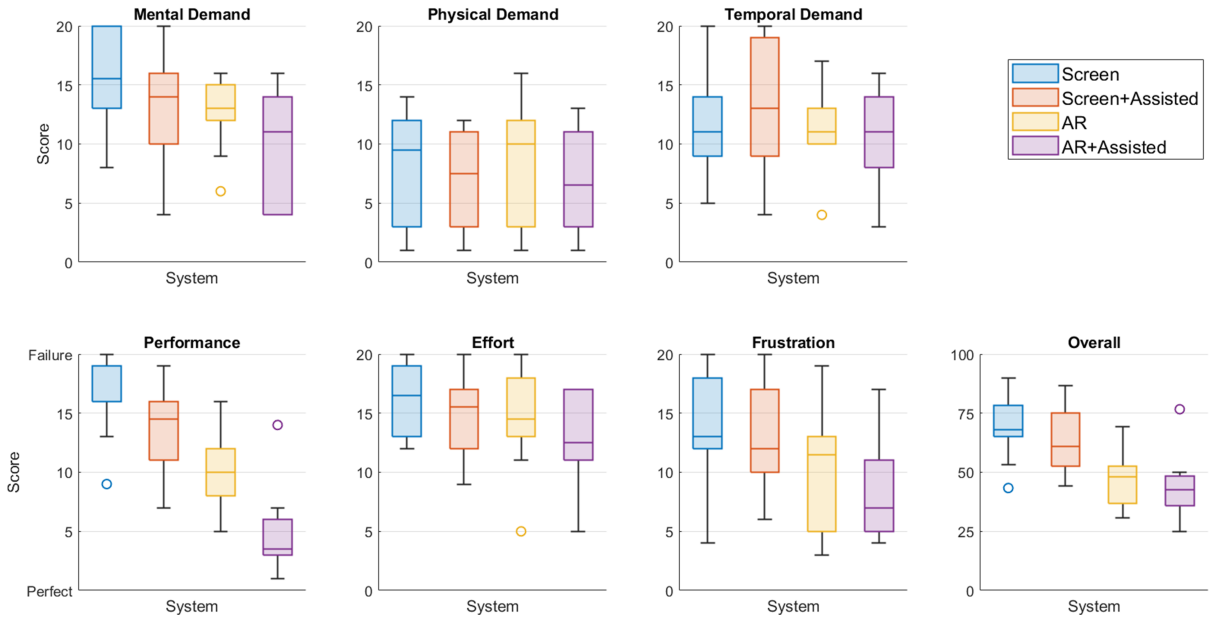

Figure 3.6: Nasa-TLX results box-plots

	Procedure setup							
	Screen		*Screen + Assisted*		*AR*		*AR + Assisted*	
Metrics	*Median*	*SD*	*Median*	*SD*	*Median*	*SD*	*Median*	*SD*
Mental demand	15.5	± 4.14	14	± 4.61	13	± 3.03	**11**	**± 4.62**
Physical demand	9.5	± 4.82	7.5	± 4.36	10	± 5.27	**6.5**	**± 4.40**
Temporal demand	11	± 4.92	13	± 6.05	**11**	**± 3.28**	11	± 4.27
Performance	19	± 3.57	14.5	± 3.75	10	± 3.82	**3.5**	**± 3.71**
Effort	16.5	± 3.00	15.5	± 3.30	14.5	± 4.35	**12.5**	**± 3.89**
Frustration	13	± 4.88	12	± 4.75	11.5	± 5.23	**7**	**± 4.79**
Overall	67.91	± 13.81	60.83	± 14.02	47.91	± 10.84	**42.5**	**± 13.73**

Table 3.3: Nasa-TLX results medians and standard deviations

p - values				
Metrics	**Setups**	*Screen + Assisted*	*AR*	*AR + Assisted*
Physical demand	*Screen*	0.5431	0.9696	0.5434
	Screen + Assisted	-	0.5929	1
	AR	-	-	0.6475
Mental demand	*Screen*	0.2872	0.1093	0.0150 (*)
	Screen + Assisted	-	0.6487	0.1366
	AR	-	-	0.1702
Temporal demand	*Screen*	0.7901	0.8787	0.7035
	Screen + Assisted	-	0.3035	0.3243
	AR	-	-	0.9391
Performance	*Screen*	0.0243 (*)	0.0023 (*)	3.0331e-04 (***)
	Screen + Assisted	-	0.1190	6.3285e-04 (***)
	AR	-	-	0.0045 (**)
Effort	*Screen*	0.5172	0.4242	0.0514
	Screen + Assisted	-	0.8199	0.1814
	AR	-	-	0.2703
Frustration	*Screen*	0.5415	0.2221	0.0407 (*)
	Screen + Assisted	-	0.4032	0.0404 (*)
	AR	-	-	0.5690
Overall	*Screen*	0.2413	0.0045 (**)	0.0032 (**)
	Screen + Assisted	-	0.0190 (*)	0.0073 (**)
	AR	-	-	0.4051

Table 3.4: Nasa-TLX p-values

3.3. Discussion and future work

In this section, the results provided above are first analyzed separately and then all together to make an overall analysis of the system performance.

3.3.1. Discussion

T and O error box-plots Here the result of Figure 3.5 are analyzed by validating the results with the test of significance provided by Table 3.1. As previously stated in section 2.4.1, the experimental validation aimed to improve the accuracy of the classical insertion needle procedure using both AR and Robotic assistance. This improvement was expected to be achieved by using the two contributions separately as well as together. The anticipated results for both the translation and orientation error were expected to show the following trends in the boxplot:

1. The combination of screen and assistance would have better results than using only the screen.
2. The use of AR in combination with assistance would have better results than using AR alone.
3. The use of AR alone would have better results than using only the screen.
4. The combination of AR and assistance would have better results than using the combination of screen and assistance.
5. The combination of AR and assistance would have better results than any of the other systems.

In this context, a "better result" refers to a smaller median error and a smaller variance in the boxplot.
By examining both the Angle and Translation error graphs in Figure 3.5, it can be seen that four out of the five expected trends listed earlier (trends 1,2,4 and 5) have been confirmed, while one has been contradicted (the point 3). Both graphs indicate a similar trend that highlights the superiority of using AR visualization in combination with robotic assistance for needle insertion accuracy. This system setup shows a significant improvement in median orientation and translation errors compared to any other system configuration, while also exhibiting lower variance.
The superiority is also supported by the p-values that indicate that this difference in the performance is not due to chance alone, p, in fact, is smaller than 0.05 for each "O error" and "T error" row in the AR Assisted column of Table 3.1 and in particular $p<0.001$ for

all the cases but one. This demonstrates that the designed system has a high level of accuracy and repeatability. In other words, the system is consistently accurate and can maintain this accuracy over multiple trials.
After analyzing the overall system performance, the boxplots for "AR" and "Screen + Assisted" can be analyzed to gain insight into the individual contributions of (i) the robotic assistance and (ii) the augmented reality visualization.

i. Robotic assistance
   In order toanalyzee the impact of robotic assistance on needle insertion accuracy one approach is to compare the boxplot of the system with robotic assistance to those without it (in particular comparing the "Screen" with the "Screen + Assisted" and the AR with the "AR + Assistance").
   It can be noticed from Table 3.1 that these p-values for both the T error and the O error are lower than 0.05 making the next analysis statistically relevant.
   This comparison reveals that both the angle and translation errors (shown in figure **??**) exhibit smaller median values in the presence of robotic assistance, indicating higher accuracy achieved with the assistance of the robot.
   Concerning the errors' variance instead, there is a higher variance in the robotic-assisted procedure compared to the "Screen" procedure. This big variance in the performance with the Robotic assistance can be given by the inexperience of the user with the robotic guidance. The user in fact, in the case the initial alignment was wrong, if the robotic guidance is active was not able to change the alignment, causing the final error to be bigger and bonding the final accuracy result to the initial alignment phase. in the free hand procedure instead, the user was able to correct the path, this led to a more repeatable accuracy result even tho the median was higher. Moreover, it can be noticed that the variance of the "AR" system is very big even though the insertion is manual but this can be due to the AR visualization modality that will be discussed below.

ii. Augmented reality visualization
   In order to compare the AR visualization methodology with respect to the 2D screen visualization, the same approach used above can be implemented. The setups with AR visualization and those without AR visualization are then compared, more specifically the comparison is between the "AR" and the "Screen" setups and between the "AR + assistance" and the "Screen + assistance" setup.
   By analyzing the orientation and translation errors, it is evident that the "AR + assistance" setup outperforms the "Screen + assistance" setup, as the former shows

significantly smaller median errors and variance in both categories (T and O). However, there is an unexpected behavior observed on the "AR" setup that shows worse performance compared to the "Screen" setup, with larger median errors and larger variance in both orientation and translation.
This unexpectedbehaviorr can be explained through the HoloLens hologram instability problem. The hologram position in fact is affected by two main problems that are also acknowledged on the Microsoft site [36]:

- Hologram Drift: a hologram appears to move away from where it was originally placed.
- Hologram Swim: When a hologram appears to sway corresponding to the motion of the user's head.

The developed system has addressed some of these issues by implementing the Dynamic registration technique (see section 2.2.3) and the holographic robot visualization, which is affected by the same drift as the path, thus making the alignment easier. However, the holographic robot and the path hologram are still subject to different "Swim" instability due to their differing relative positions with respect to the user. This can cause the user to perceive the holographic robot as moving with respect to the path when they move their head, which impacts accuracy.

Even though this instability is present, its effect on the "AR + Assisted" is minimized, as can be seen in the better result achieved with respect to the "Screen + Assistance" setup. This result can be given to the Robotic assistance contribution that lets the user focus on the alignment only at an initial moment and initial path segment, considering that then the alignment is kept from the robot along the whole insertion path. This fact is relevant because the user can perform the whole procedure of alignment with the head still and reducing the "Swim" instability.

Moreover, a final evaluation of the statistical relevance of the above considerations has to be performed. By looking at the p-values table 3.1 it can be seen that the comparison between the "AR + Assisted" and the "Screen + Assisted" setups are statistically relevant. While the p-values of the "Screen" and "AR" setups comparison are higher than 0.05 for both the translation and the orientation error. This means that all the considerations stated above are meaningful, except for the hologram instability. For this last consideration, in fact, there is not enough evidence to reject the null hypothesis of no significant difference, hence even though the translation and orientation errors boxplots show a higher variance over the "AR" setup,

there is no certainty about these results and further analysis are needed.

Execution time box-plot After analyzing the performance from the accuracy point of view, also the time has to be evaluated by looking at the "time spent" boxplot in Figure 3.5.
The first consideration that can be done is about the system implementing both AR and robotic assistance ("AR + Assistance"). It can be seen that the time spent on the performance is significantly smaller than the standard PCNL insertion technique emulated in the "Screen" setup. However, the "AR" system makes the user perform the operation significantly faster. In the end, the comparison with the "Screen + Assistance" setup enlightens a very similar distribution leading to the assumption that there is certain fixed time demand for the initial robot alignment, irrespective of the modality of visualization. The initial alignment procedure is not performed in the "AR" setup because the user has to try to be as aligned as possible along the whole path with the possibility to correct it. Nevertheless, the p-values of these boxplots have to be analyzed. By looking at the p-values table it can be seen that all the combinations are highly statistically relevant ($p<0.01$) but the "AR" to "Screen + Assistance" comparison is. For this reason, the superiority of the "AR + Assistance" setup with respect to the standard procedure is statistically relevant while the conclusion about the fixed time demand for the alignment procedure stated above needs further evaluation to be considered meaningful.

T and O error mean and standard deviation In this section, the absolute insertion accuracy error values are compared with the current state of the art in needle insertion procedure. In table 3.5 some studies regarding the state of the art of augmented reality supported needle insertion and the relative accuracy, are evaluated.
The aim of the research was to understand whether the final accuracy result of the system could be considered satisfactory compared to the current accuracy achieved from augmented reality supported needle insertion. Alongside the AR visualization also robotic assistance has been evaluated by considering whether it had been implemented or not.
Additionally, it can be noticed that while all the papers in the research concentrate on the subject of needle insertion, not all of them pertain to the PCNL procedure. Only two studies, namely [4] and [26], specifically investigate PCNL. However, the clinical applications examined in these studies are deemed comparable to PCNL in terms of needle insertion, which renders the comparison meaningful.

Upon examining the final row of Table 3.5 which displays the current work's accuracy results, it is evident that the values are quite similar to those achieved by the state

	Paper	Year	Clinical application	Hardware	Shared control	Accuracy evaluation	Accuracy
[20]	On-the-fly augmented reality for orthopedic surgery using a multimodal fiducial	2018	Fluoroscopy x-ray guidance for orthopedic surgery	Hololens and C-arm fluoroscopy machine	Free hand procedure	K-wires placed during AR-guidance vs fluoroscopy only guidance	Translation error (mean): **5.20 mm**
[22]	Augmented Reality Based Navigation for Computer Assisted Hip Resurfacing: A Proof of Concept Study	2018	Computer assisted hip resurfacing	Hololens and robotic depth camera	Free hand procedure with visual guidance and camera robot measuring the femour and the tool position online	Guide holes drilled on femour phantoms using AR guidance	Translation error (mean ± SD): **1.90 ± 0.85mm** Angular error (mean ± SD): **2.06 ± 0.89°**
[23]	Augmented reality navigation for spinal pedicle screw instrumentation using intraoperative 3D imaging	2020	Verterbral pedicle screw insertion	Hololens	Free hand procedure	Cadaver spines instrumented by pedicle screws using AR guidance and conventional guidance	Translation error (mean ± SD): **3.4 ± 1.6mm** Angular error (mean ± SD): **4.3 ± 2.3°**
[4]	Augmented Reality and Robotic-Assistance for Percutaneous Nephrolithotomy	2020	Percutaneous Nephrolithotomy	Hololens 2 and KUKA lwr4+	Virtual Fixtures applied in both allignement and insertion phase	Tooltip distance from the target center for the trasnlation. Angle between reference and real trajectories for the angle	Translation error (mean ± SD): **15.8 ± 12mm** Angular error (mean ± SD): **1.53 ± 0.54°**
[24]	Comparison of Smartphone Augmented Reality, Smartglasses Augmented Reality, and 3D CBCT-guided Fluoroscopy Navigation for Percutaneous Needle Insertion: A Phantom Study	2021	Percutaneous Needle Insertion	Hololens 1	Free hand procedure	Placement error was defined as the distance from the needle tip to the target center in a phantom procedure	Translation error (mean ± SD): **5.18 ± 3.84 mm**
[28]	An Augmented Reality-Based Interaction Scheme for Robotic Pedicle Screw Placement	2022	Pedicle screw placement	Hololens 2 and KUKA lwr4+	Robot position control with automatic positioning and drilling	Tooltip position z-axis projection and error evaluation at 3 different depth in the phantom	Translation error (mean ± SD): **3.83mm** Angular error (mean ± SD): **2.02 ± 0.6°**
[25]	Thermal Ablation of Liver Tumors Guided by Augmented Reality: An Initial Clinical Experience	2022	Thermal Ablation of Liver Tumors	Oculus Rift-S paired with a binocular camera Zed Mini for the patient registration	Free hand procedure	Real patient target to needle tip distance measured both with CT or US imaging	Translation error (mean ± SD): **3.4 ± 0.8mm**
[26]	Application of a three-dimensional visualization model in intraoperative guidance of percutaneous nephrolithotomy	2022	Percutaneous Nephrolithotomy	Hololens 2	Free hand procedure	Tooltip distance from the target center for the trasnlation.	Translation error (mean ± SD): **3.1 ± 2.9mm**
	Development of an Augmented-Reality and Robotic-Assistance application for Percutaneous Nephrolithotomy insertion proce-dure	2023	Percutaneous Nephrolithotomy	Hololens 2 and KUKA lwr4+	Robot guided needle insetrtion	Target distance from tooltip position z-axis projection and angle between refernce and real trajecotry	Translation error (mean ± SD): **3.17 ± 1.37mm** Angular error (mean ± SD): **1.24 ± 0.88°**

Table 3.5: Grey literature accuracy review

of the art. Specifically, the translation error is significantly lower than the values reported in [20], [4], [24], and [28]. It is comparable to the results reported in ,[23] ,[26] and [25] and only slightly larger than those reported in [22].
The accuracy error observed in the current work compared to the study [22] can be attributed to the inclusion of two additional features in the latter. Firstly, the study incorporates visual guidance, which changes the color of the path based on the degree of alignment. This feature provides the user with an extra means of validation, allowing them to detect errors by closing the loop of the system. Secondly, the study employs a potentially more accurate patient registration method, using point cloud registration instead of the SVD method used in the current work. While it is only an intuition, it is expected that the point cloud registration method in the study will achieve greater accuracy, as there are no registration accuracy results available in the considered study to verify this claim.
From the angular error point of view, it can be seen that the current work result is lower than [22] and [28]. This could be attributed to two distinct factors depending on the particular study being examined.
The first study does not employ any form of robotic assistance, meaning the insertion is carried out manually, which may make alignment more challenging. It should be noted that although this study exhibits greater accuracy in terms of translation error, as mentioned earlier, it still demonstrates a higher angular error. This could be due to the fact that for the user, the tip positioning is easier than the tool orientation since the tip can be kept still in position by means of the contact between the tip itself and the femur (object of the surgery in the study) while the orientation is affected from the user tiredness and hand tremor. In the end, the benefits previously mentioned, such as improved registration accuracy and visual guidance, are outbalanced by the lack of robotic assistance in reducing angular errors.

The second study instead, presents the implementation of the robotic assistance but uses a less accurate registration procedure (3.8mm of error compared to 1.6mm of the current work) that leads to a higher translation and orientation error.

Upon concluding this comparison of grey literature, it is evident that the proposed system demonstrates a level of performance on par with the best results listed above, and even outperforms some studies. Furthermore, there are opportunities to enhance the system's accuracy through the implementation of additional features, which would further improve its competitiveness.

NASA-TLX box-plots In this section, the NASA-TLX boxplots shown in figure 3.6 are interpreted alongside the median and standard deviation values in the table 3.3 and the p-values in the table 3.4. The aim of this interpretation will be to understand the system usability hence whether or not the proposed contribution brings real advantages to the user workload during the insertion procedure.

By looking at both the boxplots and the median and standard deviation values, it can be immediately seen that the "AR + Assisted" strategy stands out as the best setup in all the categories except for the time demand one (that confirms what has been seen in the execution time analyzed above).
By looking closely into every category of the NASA-TLX index the following considerations can be made.

- Mental Demand: This graph shows that both the AR modality of visualization and the robotic assistance benefits the mental demand, bringing to the conclusion that the user had a level of attention, concentration, and mental effort required to complete the task that was lowered from both the contributions.
  However, by looking at the p-values of Table 3.4 it can be seen that almost all of them are higher than 0.05 making the level of statistical relevance of this category of the NASA-TLX not meaningful. The only comparison that presents the minimum value of statistical relevance is the comparison between the "Screen" setup and the "AR + Assistance" setup. Although all the comparisons, but one, are not meaningful, it still can be stated that the proposed system requires less mental effort compared to the standard procedure used in the operating room.

- Physical Demand: This graph shows a very similar dataset for all the system setups. This behavior was expected due to the fact that all the systems implemented the manipulation of the robot, by staying in the same position and requiring roughly the same time (bringing the user to the same grade of fatigue in all the cases). All the p-values result to be higher than the statistically significant threshold of 0.05 bringing to the assumption that no conclusion can be taken.

- Temporal Demand: By looking at the graph and the related p-values (all of them bigger than 0.05) it can be said that no relevant difference can be seen between the time demand of the 4 system setups.
  This interpretation contradicts the objective measurement of the time of execution considered in the above section that enlightened time executions averages ranging from 1 min 30 sec in the best setup to 3 min in the worst one. This discrepancy can be explained by the subjective nature of the user questionnaire. In this case,

in fact, it is possible that the user didn't perceive the 1 min and 30-sec difference between the setups.
It is important to keep in mind that all the p-values are higher than 0.05 so any conclusion about these data needs further analysis.

- Performance: In this boxplot, it can be seen the clear tendency to consider both the AR visualization better than the Screen visualization and the robotic assistance better than the manual insertion. The "AR + Assistance" setup gives the perception of reaching the best performances.
  However, this tendency doesn't respect the tendency of the more objective accuracy measurement considered above. In the perception of the user in fact, the "AR" setup performs better than the "Screen + Assistance" and the "Screen" ones. This distorted perception can be given by the methodology of performance evaluation that the users were furnished with.
  The way the user was able to validate the accuracy was by checking the tool positioning on the computer screen or in the AR environment (depending on whether they were using the AR or the Screen visualization) after they performed the insertion. This validation method bonds the accuracy perception to the visualization method, that in this case, results to be more natural and clear in the AR environment with 3D perception than in a 2D Screen divided into 2 projection planes.
  All the p-values state that the performance comparisons are statistically relevant. In particular the results of the "AR + Assistance" show a p-value < 0.001 for all the comparisons making even more meaningful the higher perception the user had by using this system.
  The only p-value bigger than 0.05 is the one that relates the "Screen + Assisted" with the "AR" by making the above considerations not reliable since an actual perception of better performance with "Screen + Assisted" than with the "AR" setups (like the accuracy measurement above suggests) can still be found in further analysis.

- Effort: By looking at the boxplot graph and the relative p-values, no statistically relevant differences can be noticed between the effort put into the different system setups.
  This conclusion could be expected due to the high dependency on the "Effort" category from the "Mental Demand", "Physical Demand" and "Temporal Demand" ones. This dependency probably brought the user to apply the "Physical Demand" and "Temporal Demand" uniformity also onto the "Effort" section cutting out the difference due to the different "Mental Demand".

- Frustration: By looking at the boxplot and the p-values it can be inferred that the only meaningful difference can be seen between the "AR + Assistance" setup compared to both the "Screen" and "Screen + Assistance" setups, where the first performs better than the second two.
  This behavior can be explained by looking at the perceived "Mental Demand", "Temporal Demand" and "Performance". The frustration in fact is affected by these categories. The seen behavior could be expected because the performance and mental demand pattern is still visible even if averaged from the time demand category uniformity that makes the different setups' frustration less different.

- Overall: The last boxplot is the overall category that has been mathematically computed by merging the results over all the categories of the NASA-TLX. This last analysis is used to make more general considerations about the overall system usability.
  By looking at the overall score p-values it can be seen that there is a no statistical relevance of the comparisons between the "AR" and the "AR + Assisted" setups and the Screen and the "Screen + Assisted" setups. However, the comparison between the other categories is statistically relevant showing that the pattern of better usability of the AR systems compared to the Screen one is meaningful.

To sum up all the above considerations and create a final and more general idea about the two contributions of the work, hence the robotic assistance and AR visualization, the following general analysis is done.
In the two main performance metrics considered in the work, hence the objective measurements and the subjective user experience the AR visualization and the robotic assistance can be evaluated very differently.
In the section of objective measurement, the analysis of accuracy demonstrates a significant and beneficial effect of robot assistance on reducing translation and orientation errors. This finding is reinforced by the statistical significance shown by the p-values. Conversely, the impact of AR visualization is less prominent, unless it is used in conjunction with robot assistance.
In the section of the subjective user experience tests, the situation is reversed. The AR visualization in fact seems to create a more usable system from the user's point of view while the robotic assistance results are less intuitive to deal with.

The conclusions about the system are that, by seeing the very different behavior of the two contributions in the two different metrics, the superiority of the "AR + Assistance"

setup is explained since it shows the best results both in the user experience and in the insertion accuracy by combining both the AR visualization and the robotic assistance advantages. The goodness of the combined contributions lead also to accurate results that are comparable with the current state of the art.

3.3.2. Limitations and future work

Although the above conclusions are promising there are also some limitations and improvements that can be applied to the system that will be discussed in this section.

Limitations There are different types of limitations in the current work, and all of them can be grouped into 3 main categories:

1. Testing procedure limitations
2. HoloLens limitations
3. System design limitations

These three groups are discussed in detail in the following lines.

- Testing procedure limitations: The testing procedure is a limitation of the work because implements a methodology that can only give a preliminary indication of the advantages or the weaknesses of the system. The limiting factors are the following ones:
  - Small user group: The user test has been conducted on 14 users that repeated the test 3 times for each setup. The final dataset for each setup contained 42 measures which were revealed to be enough for a preliminary evaluation but due to the high number of statistically irrelevant comparisons (p-value > 0.05) seen in the 3.3 section a more accurate evaluation was not possible.
  - Users with no medical background: None of the users employed in the testing had a clinical background due to limited time and access to clinical partners. This fact could cause a less valid test outcome since the aim was to compare the current system with the one currently used in the operating room (OT). Furthermore, the system would be addressed to the surgeons making their opinion of the system more valuable.

  - Laboratory optimal conditions: The laboratory conditions on which the user test has been performed had the optimal not uniform background making the HoloLens positioning more accurate. This is considered a limitation because the OR background could tend to be more uniform.
  - Lack of long time ergonomic assessment: The usability of the system has been evaluated by means of the user questionnaire but due to the short time employed in the procedure only the short time comfort has been evaluated. It is worth mentioning that the operating room scenario could last for longer than 10 min, hence the time the users experienced the system. The real clinical scenario could introduce complications or further PCNL maneuver with the AR visualization and this could bring discomfort.
  - Lack of accuracy evaluation along the path: In this work, the accuracy has been evaluated only upon the final positioning. Although these results to be most important metric, the accuracy could be further analyzed along the path. By doing so, the whole insertion pathway would be evaluated by further understanding the safety of the fragile structures surrounding the pre-planned path. This metric would have a bigger impact on the manual insertion procedures evaluated since the path correction employed by the users once entered in the manikin would be detected and considered.

- HoloLens limitations: Another big limitation of the current work are the HoloLens. In fact, although the results are promising there are some behaviors asked to the user during the AR insertion procedure that could create discomfort to the surgeon and badly impact the surgery outcomes. The HoloLens limitations are the following ones:
  - Hologram Drift problem: The HoloLens drift problem, hence the movement of the holograms from their initial position over time, is a big topic because heavily impacts the workflow of the procedure. The concept has already been introduced in the section 2.2.3. The current work tries to address the problem by implementing dynamic registration in order to implement the hologram drift correction in the less intrusive way and in order to reduce the workflow interruption to the minimum. However, even though the interruption is minimized, it is still present.
  - Hologram Swim problem: The hologram swim problem has already been mentioned when discussing the accuracy error of the AR setup compared to the Screen setup. This problem is the hologram movement that happens when the

user's head moves. This is behavior is caused by the HoloLens re-rendering of the hologram in order to adapt to the new user viewpoint.
The result of the hologram swim problem is a big increase in difficulty in the alignment performance.
In order to reduce this problem the users were asked to move the head as little as possible when evaluating the alignment to the path. This request may be more difficult for a surgeon to accept.

- HoloLens depth sensing: The last HoloLens limitation is the depth sensing. As has been mentioned in the study [33], the instability of the HoloLens depth sensing causes the introduction of a 3.38mm deviation to the hologram position every 70cm of distance the user has from the hologram. This leads to the conclusion that the closer the user is to the path, the more accurate the positioning is.
  Just like the Swim problem above, the users were asked to modify their behavior in a way to be as close as possible to the patient model. Again this request may be more difficult for a surgeon to accept due to the bigger viewing field needed for him to perform the overall surgical procedure.

- System design limitations: The last group of limitations is the one related to the system design limitation. Although the final accuracy results are promising there are some aspects of the system that suffer from some problems. The problems are the following one:

  - High complexity of the system: In order to increase the accuracy, the presented system implements many modules. In fact, the system hardware is mainly formed by: an Optical Tracker, a KUKA robot, the HoloLens, and a Computer. This setup is a much more complex setup compared to the system currently used in the OR that implements only the C-arm for the fluoroscopy. Moreover, the system complexity is even higher than other AR supported needle insertion systems found in the grey literature such as [4] that don't implements the Optical Tracker or [26] that doesn't implement a robot.
    The more complex systems are disadvantageous with respect to the more simple one since the presence of more modules could make the user learn slower, the system cost higher and the system robustness worse.

  - Optical Tracker implementation: The Optical Tracker implementation is a big advantage for the phantom to robot registration because it implements a really accurate measurement tool by obtaining a very good registration accuracy (See

section 2.2.2). However, the OT implements some limitations with respect to the usage of the HoloLens QR code tracking system such as the higher cost of the device and the complexity of the procedure.

Future works In the end, the possible future works are discussed in order to outline potential areas of research that could improve the impact of the study. In particular, the above-mentioned limitations have been analyzed in order to build the possible future works that due to lack of resources or time have not been implemented. The possible future works could be the following ones:

- Expert users: The experimental validation can be conducted with the help of surgeons that could more clearly indicate the system limitations with respect to a possible real operating room scenario application.
- OR emulation: The laboratory could be made as similar as possible to an OR in order to test the HoloLens spatial awareness feature in this scenario.
- Accuracy assessment along the path: The Accuracy could be evaluated also along the path of insertion by reading the */pose/Tool_tip* ROS topic during the insertion and saving it as a discrete sequence of positions.
  The system is already configured to make this acquisition because it implements the same logic to acquire the insertion final position in the user study mentioned above.
- Automatic dynamic registration: The Dynamic registration procedure that has already been implemented can be further improved. In fact, this feature has been designed in order to reduce workflow interruption, an objective that has been achieved. The following step would be to completely delete the workflow interruption by creating a totally automatic dynamic registration. The idea could be to substitute the dynamic registration button implemented in this work with an automatic algorithm that, by comparing the scanned QR code position with respect to the hologram position, can detect the hologram drift and apply the correction.
- Visual guidance: As the study [22] demonstrates, a possible improvement in the insertion accuracy can be reached by implementing the visual guidance, hence a light feedback to the user that is able to understand the goodness of the alignment by seeing the path color. The path would be green in the case of alignment error within a certain interval and red in the case it is outside.
- Alignment virtual fixtures: Another possible improvement could be given by the implementation of virtual fixtures for the alignment step. This concept has been implemented in the study [4]. The implementation of the virtual fixtures could make

the alignment even more accurate by keeping a certain degree of freedom for the surgeon in case of need.

- Breathing compensation: A big problem in the needle insertion procedure systems is the compensation of the patient's breathing movement. The current work, in fact, without compensation of the breathing would make the surgeon strictly follow a fixed path that actually would be moving, causing insertion accuracy to get much lower and risking harming the patient. The possible application in the operating room of the current work must consider this aspect.

Bibliography

[1] Raymond Ko, Frédéric Soucy, John D Denstedt, and Hassan Razvi. Percutaneous nephrolithotomy made easier: a practical guide, tips and tricks. *BJU international*, 101(5):535–539, 2008.

[2] Hsieh-Yu Li, Ishara Paranawithana, Zhong Hoo Chau, Liangjing Yang, Terence Sey Kiat Lim, Shaohui Foong, Foo Cheong Ng, and U-Xuan Tan. Towards to a robotic assisted system for percutaneous nephrolithotomy. In *2018 IEEE/RSJ International Conference on Intelligent Robots and Systems (IROS)*, pages 791–797. IEEE, 2018.

[3] Sutchin R Patel and Stephen Y Nakada. The modern history and evolution of percutaneous nephrolithotomy. *Journal of endourology*, 29(2):153–157, 2015.

[4] Federica Ferraguti, Marco Minelli, Saverio Farsoni, Stefano Bazzani, Marcello Bonfè, Alexandre Vandanjon, Stefano Puliatti, Giampaolo Bianchi, and Cristian Secchi. Augmented reality and robotic-assistance for percutaneous nephrolithotomy. *IEEE robotics and automation letters*, 5(3):4556–4563, 2020.

[5] Li-Ming Su, Dan Stoianovici, Thomas W Jarrett, Alexandru Patriciu, William W Roberts, Jeffrey A Cadeddu, Sanjay Ramakumar, Stephen B Solomon, and Louis R Kavoussi. Robotic percutaneous access to the kidney: comparison with standard manual access. *Journal of Endourology*, 16(7):471–475, 2002.

[6] Seyed Amir Mohsen Ziaee, Mehrdad Mohammadi Sichani, Amir Hossein Kashi, and Mohammad Samzadeh. Evaluation of the learning curve for percutaneous nephrolithotomy. *Urology Journal*, 7(4):226–231, 2010.

[7] Brian S Peters, Priscila R Armijo, Crystal Krause, Songita A Choudhury, and Dmitry Oleynikov. Review of emerging surgical robotic technology. *Surgical endoscopy*, 32:1636–1655, 2018.

[8] Eleonora Barcali, Ernesto Iadanza, Leonardo Manetti, Piergiorgio Francia, Cosimo Nardi, and Leonardo Bocchi. Augmented reality in surgery: A scoping review. *Applied Sciences*, 12(14):6890, 2022.

[9] Zhanat Makhataeva and Huseyin Atakan Varol. Augmented reality for robotics: A review. *Robotics*, 9(2):21, 2020.

[10] Jens J Rassweiler, Michael Müller, Markus Fangerau, Jan Klein, Ali S Goezen, Philippe Pereira, Hans-Peter Meinzer, and Dogu Teber. ipad-assisted percutaneous access to the kidney using marker-based navigation: initial clinical experience. *European urology*, 61(3):628–631, 2011.

[11] Yifan Chang, Xiaojun Lu, Qingliang Zhu, Chuanliang Xu, Yinghao Sun, and Shancheng Ren. Single-port transperitoneal robotic-assisted laparoscopic radical prostatectomy (spralp): initial experience. *Asian Journal of Urology*, 6(3):294–297, 2019.

[12] SJ Phee, KY Ho, D Lomanto, SC Low, VA Huynh, AP Kencana, K Yang, ZL Sun, and SC Sydney Chung. Natural orifice transgastric endoscopic wedge hepatic resection in an experimental model using an intuitively controlled master and slave transluminal endoscopic robot (master). *Surgical endoscopy*, 24:2293–2298, 2010.

[13] Aydin Aktas, Erman Aytac, Mustafa Bas, Orgun Gunes, Serim Hande Tarcan, Eren Esen, Cihan Gokler, Afag Aghayeva, Ufuk Uylas, Volkan Ozben, et al. Totally minimally invasive radical gastrectomy with the da vinci xi® robotic system versus straight laparoscopy for gastric adenocarcinoma. *The International Journal of Medical Robotics and Computer Assisted Surgery*, 16(6):1–9, 2020.

[14] Khurshid R Ghani, Craig G Rogers, Akshay Sood, Ramesh Kumar, Michael Ehlert, Wooju Jeong, Arvind Ganpule, Mahendra Bhandari, Mahesh Desai, and Mani Menon. Robot-assisted anatrophic nephrolithotomy with renal hypothermia for managing staghorn calculi. *Journal of endourology*, 27(11):1393–1398, 2013.

[15] Olivia Wilz, Ben Sainsbury, and Carlos Rossa. Constrained haptic-guided shared control for collaborative human–robot percutaneous nephrolithotomy training. *Mechatronics*, 75:102528, 2021.

[16] Dan Stoianovici, Louis L Whitcomb, James H Anderson, Russell H Taylor, and Louis R Kavoussi. A modular surgical robotic system for image guided percutaneous procedures. In *Medical Image Computing and Computer-Assisted Intervention—MICCAI'98: First International Conference Cambridge, MA, USA, October 11–13, 1998 Proceedings 1*, pages 404–410. Springer, 1998.

[17] Dan Stoianovici, Changhan Jun, Sunghwan Lim, Pan Li, Doru Petrisor, Stanley Fricke, Karun Sharma, and Kevin Cleary. Multi-imager compatible, mr safe, remote

center of motion needle-guide robot. *IEEE Transactions on Biomedical Engineering*, 65(1):165–177, 2017.

[18] Zachary G Schwam, Vivian F Kaul, Daniel D Bu, Alfred-Marc Calo Iloreta, Joshua B Bederson, Enrique Perez, Maura K Cosetti, and George B Wanna. The utility of augmented reality in lateral skull base surgery: a preliminary report. *American Journal of Otolaryngology*, 42(4):102942, 2021.

[19] Ganesh Shrestha, Abeer Alsadoon, PWC Prasad, Thair Al-Dala'in, and Ahmad Alrubaie. A novel enhanced energy function using augmented reality for a bowel: modified region and weighted factor. *Multimedia Tools and Applications*, 80:17893–17922, 2021.

[20] Sebastian Andress, Alex Johnson, Mathias Unberath, Alexander Felix Winkler, Kevin Yu, Javad Fotouhi, Simon Weidert, Greg Osgood, and Nassir Navab. On-the-fly augmented reality for orthopedic surgery using a multimodal fiducial. *Journal of Medical Imaging*, 5(2):021209–021209, 2018.

[21] Hai-Su Tao, Jin-Yu Lin, Wang Luo, Rui Chen, Wen Zhu, Chi-Hua Fang, and Jian Yang. Application of real-time augmented reality laparoscopic navigation in splenectomy for massive splenomegaly. *World Journal of Surgery*, 45:2108–2115, 2021.

[22] He Liu, Edouard Auvinet, Joshua Giles, and Ferdinando Rodriguez y Baena. Augmented reality based navigation for computer assisted hip resurfacing: a proof of concept study. *Annals of biomedical engineering*, 46:1595–1605, 2018.

[23] Fabio Müller, Simon Roner, Florentin Liebmann, José M Spirig, Philipp Fürnstahl, and Mazda Farshad. Augmented reality navigation for spinal pedicle screw instrumentation using intraoperative 3d imaging. *The Spine Journal*, 20(4):621–628, 2020.

[24] Dilara J Long, Ming Li, Quirina MB De Ruiter, Rachel Hecht, Xiaobai Li, Nicole Varble, Maxime Blain, Michael T Kassin, Karun V Sharma, Shawn Sarin, et al. Comparison of smartphone augmented reality, smartglasses augmented reality, and 3d cbct-guided fluoroscopy navigation for percutaneous needle insertion: a phantom study. *CardioVascular and Interventional Radiology*, 44:774–781, 2021.

[25] Marco Solbiati, Tiziana Ierace, Riccardo Muglia, Vittorio Pedicini, Roberto Iezzi, Katia M Passera, Alessandro C Rotilio, S Nahum Goldberg, and Luigi A Solbiati. Thermal ablation of liver tumors guided by augmented reality: an initial clinical experience. *Cancers*, 14(5):1312, 2022.

[26] Lei Wang, Zichen Zhao, Gang Wang, Jianfang Zhou, He Zhu, Hongfeng Guo, Hua-

gang Huang, Mingchuan Yu, Gang Zhu, Ningchen Li, et al. Application of a three-dimensional visualization model in intraoperative guidance of percutaneous nephrolithotomy. *International Journal of Urology*, 29(8):838–844, 2022.

[27] Federica Ferraguti, Saverio Farsoni, and Marcello Bonfè. Augmented reality and robotic systems for assistance in percutaneous nephrolithotomy procedures: Recent advances and future perspectives. *Electronics*, 11(19):2984, 2022.

[28] Viktor Vörös, Ruixuan Li, Ayoob Davoodi, Gauthier Wybaillie, Emmanuel Vander Poorten, and Kenan Niu. An augmented reality-based interaction scheme for robotic pedicle screw placement. *Journal of Imaging*, 8(10):273, 2022.

[29] Puxun Tu, Chunxia Qin, Yan Guo, Dongyuan Li, Abel J Lungu, Huixiang Wang, and Xiaojun Chen. Ultrasound image guided and mixed reality-based surgical system with real-time soft tissue deformation computing for robotic cervical pedicle screw placement. *IEEE Transactions on Biomedical Engineering*, 69(8):2593–2603, 2022.

[30] Wenyuan Sun, Jihao Liu, Yuyun Zhao, and Guoyan Zheng. A novel point set registration-based hand–eye calibration method for robot-assisted surgery. *Sensors*, 22(21):8446, 2022.

[31] Junling Fu, Qingsheng Liu Maria Chiara Palumbo, Elisa Iovene, Alberto Redaelli Ilaria Burzo, Giancarlo Ferrigno, and Elena De Momi. Augmented reality-assisted robot learning framework for minimally invasive surgery task. *IEEE International Conference on Robotics and Automation (ICRA), London 2023*.

[32] K Somani Arun, Thomas S Huang, and Steven D Blostein. Least-squares fitting of two 3-d point sets. *IEEE Transactions on pattern analysis and machine intelligence*, (5):698–700, 1987.

[33] Wenhao Gu, Kinjal Shah, Jonathan Knopf, Nassir Navab, and Mathias Unberath. Feasibility of image-based augmented reality guidance of total shoulder arthroplasty using microsoft hololens 1. *Computer Methods in Biomechanics and Biomedical Engineering: Imaging & Visualization*, 9(3):261–270, 2021.

[34] Maria Chiara Palumbo, Simone Saitta, Marco Schiariti, Maria Chiara Sbarra, Eleonora Turconi, Gabriella Raccuia, Junling Fu, Villiam Dallolio, Paolo Ferroli, Emiliano Votta, et al. Mixed reality and deep learning for external ventricular drainage placement: A fast and automatic workflow for emergency treatments. In *Medical Image Computing and Computer Assisted Intervention–MICCAI 2022: 25th International Conference, Singapore, September 18–22, 2022, Proceedings, Part VII*, pages 147–156. Springer, 2022.

[35] Maria C Palumbo, Laura Morchi, Valentina Corbetta, Arianna Menciassi, Elena De Momi, Emiliano Votta, and Alberto Redaelli. An easy and user independent augmented reality based navigation system for radiation-free interventional procedure. In *2022 International Symposium on Medical Robotics (ISMR)*, pages 1–7. IEEE, 2022.

[36] Microsoft. Hologram stability. `https://learn.microsoft.com/en-us/windows/mixed-reality/develop/advanced-concepts/hologram-stability`, 2021.

A | Appendix

List of Figures

List of Tables